ADDITIVE MANUFACTURING OF OPTICALLY TRANSPARENT GLASS

JOHN KLEIN
BACHELOR OF ARCHITECTURE
SOUTHERN CALIFORNIA INSTITUTE OF ARCHITECTURE (SCI-ARC 2010)

Submitted to the Program in Media Arts and Sciences, School of Architecture and Planning, in partial fulfillment of the requirements for the degree of

Master of Science
at the

MASSACHUSETTS INSTITUTE OF TECHNOLOGY

September 2015

Author Signature redacted
John Klein
Program in Media Arts and Sciences
August 7, 2015

Certified by Signature redacted
Professor Neri Oxman
Associate Professor of Media Art and Sciences
Thesis Advisor

Accepted by Signature redacted
Professor Patricia Maes
Associate Academic Head
Program in Media Arts and Sciences

ADDITIVE MANUFACTURING OF OPTICALLY TRANSPARENT GLASS

JOHN KLEIN

Submitted to the Program in Media Arts and Sciences, School of Architecture and Planning, on August 7, 2015, in partial fulfillment of the requirements for the degree of Master of Science

ABSTRACT

The thesis presents an *Additive Manufacturing Enabling Technology for Optically Transparent Glass*. The platform builds on existing manufacturing traditions and introduces new dimensions of novelty across scales by producing unique structures with numerous potential applications in product-, and architectural-design. The platform is comprised of scalable modular elements able to operate at the high temperatures required to process glass from a molten state to an annealed product. The process demonstrated enables the construction of 3D parts as described by Computer Aided Design (CAD) models. Processing parameters such as temperature, flow rate, layer height and feed rate, can be adjusted to tailor the printing process to the desired component; its shape and its properties. The research explores, defines and hard-codes geometric constraints and coiling patterns as well as the integration of various colors into the current controllable process, contributing to a new design and manufacturing space. Performed characterization of the printed material to determine its morphological, mechanical and optical properties, is presented and discussed. Printed parts demonstrated strong adhesion between layers and satisfying optical clarity. The molten glass 3D printer as well as the fabricated objects exhibited, demonstrate the production of parts which are highly repeatable, enable light transmission, and resemble the visual and mechanical performance of glass constructs that are conventionally obtained. Utilizing the optical nature of glass, complex caustic patterns were created by projecting light through the printed objects. The 3D printed glass objects and process described here, aim to contribute new capabilities to the ever-evolving history of a very challenging but limitless material – *glass*.

Thesis advisor:
Professor Neri Oxman
Title: Associate Professor, MIT Program in Media Arts and Sciences

ADDITIVE MANUFACTURING OF OPTICALLY TRANSPARENT GLASS

JOHN KLEIN

Submitted to the Program in Media Arts and Sciences in partial fulfillment of the requirements for the degree of Master of Science in Media Arts and Sciences

Signature redacted

J. Meejin Yoon
Head of the Department of Architecture
Massachusetts Institute of Technology
Thesis Reader

ADDITIVE MANUFACTURING OF OPTICALLY TRANSPARENT GLASS

JOHN KLEIN

Submitted to the Program in Media Arts and Sciences in partial fulfillment of the requirements for the degree of Master of Science in Media Arts and Sciences

Signature redacted

Professor Neil Gershenfeld
Director, Center for Bits and Atoms
Massachusetts Institute of Technology
Thesis Reader

ACKNOWLEDGMENTS

First and foremost, I would like to thank one of the most influential people in my life whom I'm privileged to have as a mentor: Neri Oxman. Neri thank you for all your support and encouragement over the last two years, my experience in the Mediated Matter Group has changed the way I think and see the world.

Meejin Yoon, thank you for providing the architectural framework through our meetings and conversations, which guided the way I structured my work in the Media Lab. Your practice is one I aspire to as an architect.

Neil Gershenfeld, thank you for your guidance and encouragement throughout my time here at MIT. My most enjoyable memories are from my time down in the Center for Bits and Atoms, and your way of thinking about making has left a permanent mark on me.

John Ochsendorf, it has been an honor to engage with you here at MIT, as your work was one of the reasons which drew me into the community. I look forward to collaborating together on the large scale glass structure!

Peter Houk, not only have you and the MIT Glass Lab been an incredible source of inspiration for my thesis, you have always been someone I could reach out to at any time and count on. It has been a true pleasure to collaborate together over the last 2 years.

Markus Kayser, out of all the people in the Mediated Matter Group, I've worked together closely with you over the last two years. Thank you for making this experience one of the most intellectually stimulating periods of my life. I've never met anyone who has such a unique way of perceiving the world. Your work on the solar sinter had set the tone for my interests in the group, and I'm confident we will continue to collaborate for years to come.

Chikara Inamura, we've worked together now in Asia, Europe and America for over 10 years, and every project that we put our heads together has turned out to be my best work. I very much look forward to kicking off the next season of I|K.

Will Patrick, you and I entered the MIT journey together trapped in a small remote office, and built a genuine friendship through our curiosities that blended design and engineering.

Steven Keating, not only have you made me step out of every comfort zone I've ever built prior to joining the group, the strength and courage I witnessed through you will stay with me for the rest of my life. Thank you for pushing me to technically challenge myself in ways I never

thought I could achieve, and thank you for your generous gifts of maple syrup from your hometown in Canada.

Giorgia Franchin, thank you for joining the Mediated Matter Group and being my partner in crime on the glass printing project. I've been fortunate to share this unique, close collaboration, between a material scientist and an architect, and this has proved to be one of my most valuable experiences here at MIT.

Kelly Donovan, thank you for everything you have done for me throughout my time in Mediated Matter Group! Your support, guidance, advice and retreats to the Rebel Ranch Horse Farm made my MIT experience possible.

Sunanda Sharma, Jorge Duro-Royo, Laia Mogas-Soldevila, Daniel Lizardo, thank you all for your comradery and friendship. I couldn't have asked to work with a more talented group of individuals over the last two years.

James Weaver, your inspiration and knowledge about the entire world is simply unprecedented. Thank you for all the meetings at your office in the WYSS to discuss the exciting intersection of materials and biology. You are truly one of a kind.

Will Langford, thank you for all the fabrication, material, physics, mechanical, electrical, robotic, cooking and baking knowledge you have shared with my over the last two years! Your always are a genuine source of inspiration for me and I very much value our friendship.

Michael Stern, the collaboration with you over the past two years has not only been incredibly fruitful, but you have changed the way that I approach design. It is very rare that an architect and mechanical engineer work together at such a "high bandwidth", and your sense of pragmatic logical thinking grounded my work and made the G3P project come together.

Erik & Marty Demaine, thank you for your support and sense of humor in the glass lab when things would catastrophically go wrong. Your jokes and playful spirits always put a smile on the team's faces when we were in need.

John DiFrancesco, Tom Lutz and Seth Cimarron Avecilla, thank you all for all the support down in the Fab Lab. As you could probably tell by the amount of hours I spent in the shop, it is my most favorite space in all of MIT. Thank you for supporting every project I brought down, and your willingness to help me realize my visions.

Kevin Davis, Cornelle King and Jessica Tsymbal, thank you three for all your efforts and support in helping our team realize the MIT Media Lab "Glass" Exhibition. Your dedication, and

do-whatever-it-takes attitude to ensure quality projects, has enabled our group to grow through each exhibition.

Linda Peterson, Keira Horowitz, thank you both for all your help during my time here in the MIT Media Lab. Your willingness to always look after our whole cohort and take the time to make sure that I am on track is greatly appreciated.

Corning Incorporated, thank you for inspiring and hosting our team in Corning's headquarters, Sullivan Park and the Corning Museum of Glass. I've learned an incredible amount of knowledge about the rich history of glass through the trip that has greatly influenced my thesis.

Lorna Gibson, thank you for opening my eyes to the incredible world of material science. Your course was - hands down - the most challenging experience I've ever went through in my entire life. It was also equally the most rewarding. Thank you for all your support taking the time to sit in your office to share your knowledge and passion.

I'd like to thank Zaha Hadid and Patrik Schumacher for all the incredible opportunities you provided me during my five years at ZHA. Thank you for believing in me, and not thinking twice to throw me in the fire(s) all over the world.

I'd, also like to thank the highly influential people who shaped my career as an architect: Cristiano Ceccato, Satoshi Ohashi, Armando Solano, Michael Grau, Shajay Bhooshan, Eric Owen Moss, Marcelo Spina, Peter Testa, Elena Manferdini, Alexis Rochas, Mark Burry, Jane Bury, David Gerber, Sanford Kwinter and Steven Cohen.

Last, but far from least, I would like to thank my family. I cannot even begin to express how thankful I am to everyone and how grateful I am to have come from such a genuine group of people. Thank you for everything you have ever done for me and all your encouragement. This thesis is dedicated to all of you.

CONTENTS

LIST OF FIGURES

LIST OF TABLES

1

INTRODUCTION & BACKGROUND

1.1. GLASS

1.1.1. HISTORY & CONTEXT

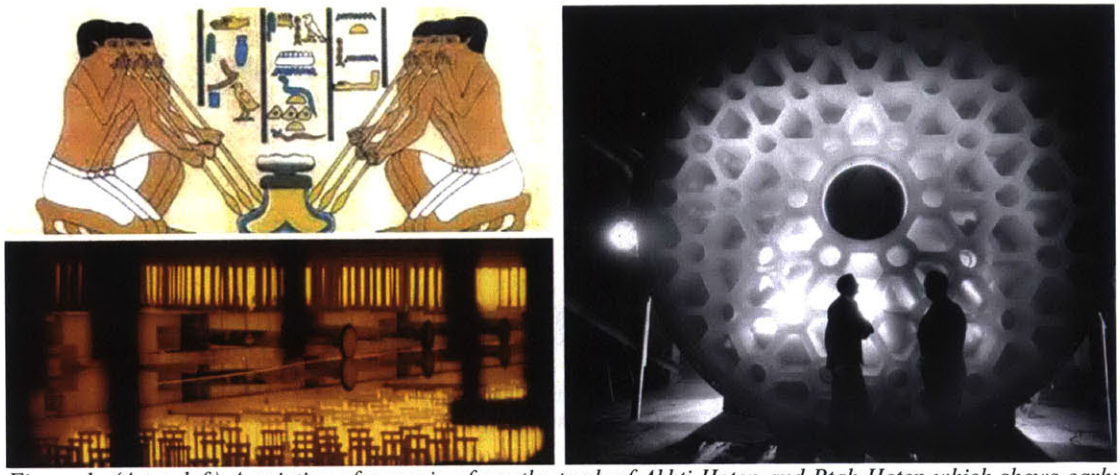

Figure 1: (A-top left) A painting of a carving from the tomb of Akhti-Hotep and Ptah-Hotep which shows early Egyptian glass blowing. Image source: Italmole S.N.C (B-bottom left) Pilkington float glass process. Image source: Corning Museum of Glass (C-right) Hale telescope at Palomar Observatory made from Pyrex. Image source: Corning Museum of Glass

Ancient yet modern, enclosing yet invisible, glass was first created in Mesopotamia and Ancient Egypt 4,500 years ago. Precise recipes for its production - the chemistry and techniques - often remain guarded secrets. Glass can be molded, formed, blown, plated or sintered; its formal qualities are closely tied to techniques used for its formation.

The story of glass is largely about people overcoming limitations imposed by substantial difficulties inherent in the material itself. Among these difficulties are achieving and sustaining the elevated temperatures necessary to melt and form glass, developing methods of forming glass without being able to touch it with the human hand, and the problem of thermal shock (resulting in cracking or catastrophic failure).

From the discovery of the core-forming process for bead-making in ancient Egypt (Figure 1A), to the invention of the metal blow pipe during Roman times, to the modern industrial Pilkington process for making large-scale flat glass (Figure 1B), to lenses that enabled human kind to see down into the petri dish and out into the universe (Figure 1C), and to the drawn

fibers that revolutionized the way humans communicate across the planet, each new breakthrough in glass technology occurred as a result of prolonged experimentation and ingenuity, and has given rise to a new universe of possibilities for uses of the material.

The thesis presents an *Additive Manufacturing Enabling Technology for Optically Transparent Glass*, which builds on existing manufacturing traditions and introduces new dimensions of novelty across scales by producing unique structures with numerous potential applications in product, and architectural design.

In other words, the thesis aims to contribute to a quantum context - ever-evolving, constantly breaking through limitations in order to discover new capabilities of this very challenging but limitless material.

1.1.2. PROPERTIES OF GLASS

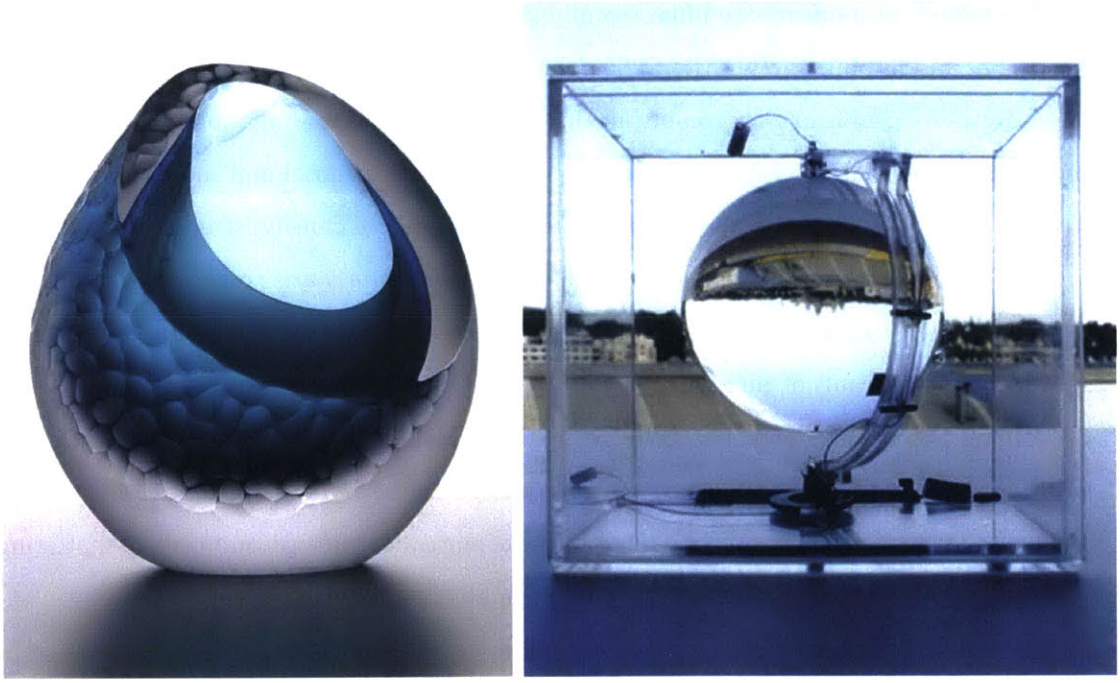

Figure 2: (A-left) Artist Joanne Mitchell's sculptural glass design. Image source: North East Art Collective (B-right) André Broessel's spherical solar concentrators. Image source: Inhabitat weblog

Glass continuously converts into liquid upon heating, and has an amorphous structure with a random molecular organization[39, 41]. Soda-lime glass (a form of glass that is used world-wide) is primarily obtained from the melting of ±70% sand (silica), ±15% soda ash (sodium carbonate)

and ±5% limestone (calcium carbonate) [39, 41]. This raw material mixture is commonly referred to as "batch," and has not changed dramatically since the Egyptians[39].

Glass' random molecular structure impacts its material behavior under different temperatures. Soda-lime glass has a working range between 1000°F - 1700°F which enables a slow transition from a solid to a liquid state[39]. This working range enables glass to have its unique forming capabilities such as molding, slumping, fusing and blowing[39].

Since glass is an inert chemically stable substance (in its application environment) with high durability it is manufactured in large volumes as containers, vessels and laboratory equipment for the food and drug industry to prevent contamination to sensitive products.

Glass' capacity to refract and reflect light give it very appealing optical properties (Figure 2A) [41]. When light travels through glass that is formed into different convex and concave geometries, it will deviate (refract), and focus, which causes the formed glass to exhibit properties of optical magnification (Figure 2B) [37].

Electronic components are often integrated with glass, due its good electrical insulation properties and its ability to withstand heat.

A property profile of glass can be seen in (Figure 3) which shows the specific values for the mechanical, thermal, electrical and eco properties (for the material and molding processes). Three Ashby charts are also shown to situate the strength vs density, strength vs toughness and energy content vs cost against other material classes. The charts show that while glass is brittle with very little toughness, it has a higher compressive strength than concrete, and requires large amounts of energy for its forming and shaping processes[34].

Chemical processes and composites were developed over the 20th to further augment the properties and performance of glass such glass and polymer laminations (for safety glass), heat treating and chemical tempering (to increase the compressive strength and control shattering), and tin oxide coatings (to allow light to pass through but not heat) [37].

As a result of glass' material properties, and advances in manufacturing process, it has made its way into numerous industries with varying applications. Most notable are the architectural, automotive, aerospace and medical industries.

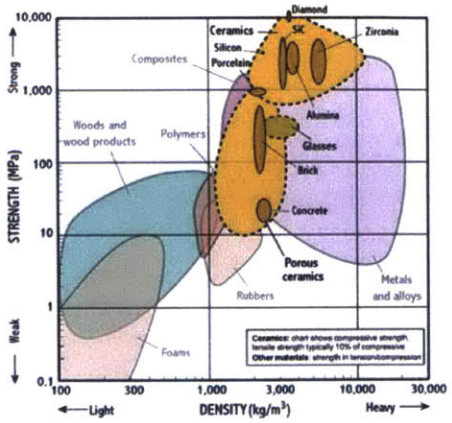

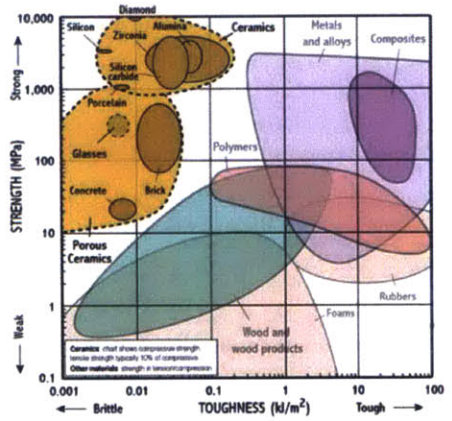

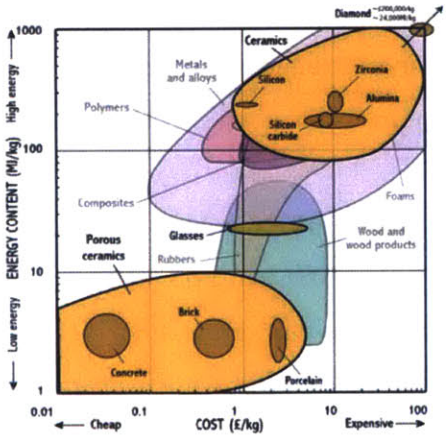

General properties	Values	Units
Density	2,400 – 2,490	Kg/m^3
Price	0.8 – 1.7	USD/kg
Mechanical properties		
Young's modulus	68 – 72	GPa
Yield strength	30 – 35	MPa
Tensile strength	31 – 35	MPa
Elongation	0	%
Hardness – Vickers	439 - 484	HV
Fatigue strength (10^7 c)	29.4 – 32.5	MPa
Fracture toughness	0.55 – 0.7	$MPa \cdot m^{1/2}$
Thermal properties		
Max. service temp.	443 - 673	K
T. conductor or insulator	Poor insulator	
T. conductivity	0.7 – 1.3	$W/m \cdot K$
Specific heat capacity	850 - 950	$J/kg \cdot K$
T. expansion coefficient	9.1 – 9.5	μstrain/°C
Electrical properties		
E. conductor or insulator	Good insulator	
Electrical resistivity	$7.9x10^{17}$ - $7.9x10^{18}$	$\mu ohm \cdot cm$
Dielectric constant	7 – 7.6	
Dielectric strength	12 - 14	10^6 V/m
Eco properties: material		
Global production	84×10^6	m. ton / yr
Reserves	1×10^{12}	m. ton
Embodied energy	10 - 11	MJ/kg
CO_2 footprint	0.7 – 0.8	Kg/kg
Water usage	14 – 20.5	L/kg
Eco-indicator	75	millipoints/kg
Eco properties: processing		
Glass molding energy	8.2 – 9.2	MJ/kg
Glass molding CO_2	0.66 – 0.73	kg/kg
End of life		
Embodied energy recycling	7.4 – 9.0	MJ/kg
CO_2 footprint recycling	0.44 – 0.54	kg/kg
Recycle fraction in supply	22 - 26	%

Figure 3: Ashby Charts (top left) Strength vs Density (middle left) Strength vs Toughness (bottom left) Energy Content vs Cost. Image source: University of Cambridge, Department of Engineering (right) Soda-lime glass material profile. Table source: Materials and the Environment[34]

1.1.3. GLASS APPLICATIONS & ADVANCES

1.1.3.1. ARCHITECTURAL WINDOWS

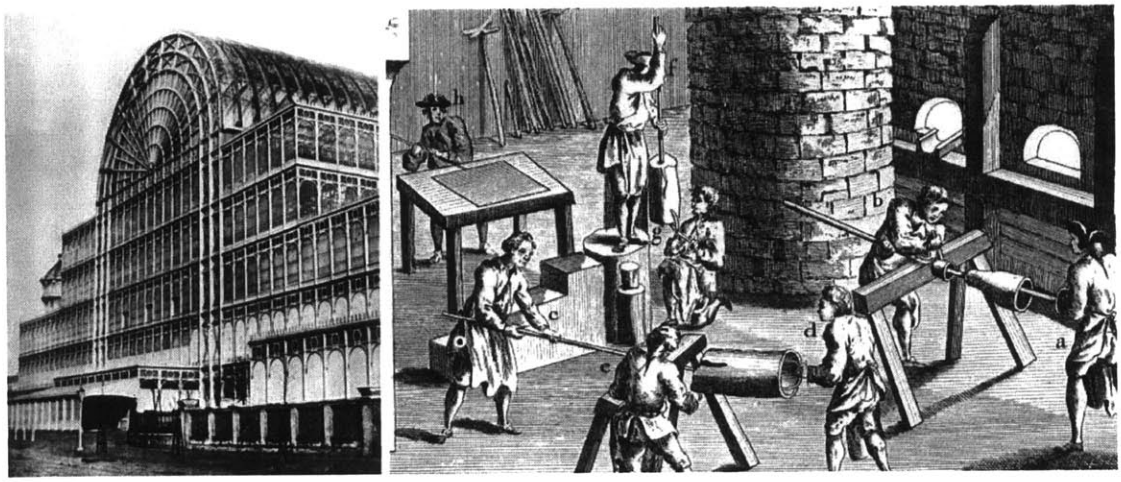

Figure 4: (A-left) Front view of the Crystal Palace in London. Image source: Former Days (B-right) Rendition of a glass factory forming cylindrical glass tubes for window applications. Image source: Diderot Encyclopedia, Glass

Windows have been a fundamental architectural design feature as early as the Romans, and function to establish relationships with the building's interior and exterior volumes, and let light, heat and air indoors. It is inevitable that glass has been a sought out material choice for windows given its optical properties and durability. Advances in building and manufacturing technology enabled windows to evolve from fenestrations in architectural envelopes to entire transparent building skins.

One of the most notable architectural-engineering glass building precedents is the Crystal Palace (Figure 4A), which was constructed in 1851 in Hyde Park, London. Prior to this project, glass panes were manufactured through a technique of blowing large glass bubbles, then rotating them to form a flat pane (also known as a crown)[37]. The crowns were then annealed and subdivided into rectangular window panes[37].

The Crystal Palace used an alternative technique to make its 300,000 glass panes bigger, which involved swinging a large glass bubble instead of spinning it, to form long cylindrical tubes (Figure 4B)[37]. The tubes were then sheared and unrolled flat, or curved to form the glass enclosure for the Palace[37]. This was an intensive and laborious manual process[37].

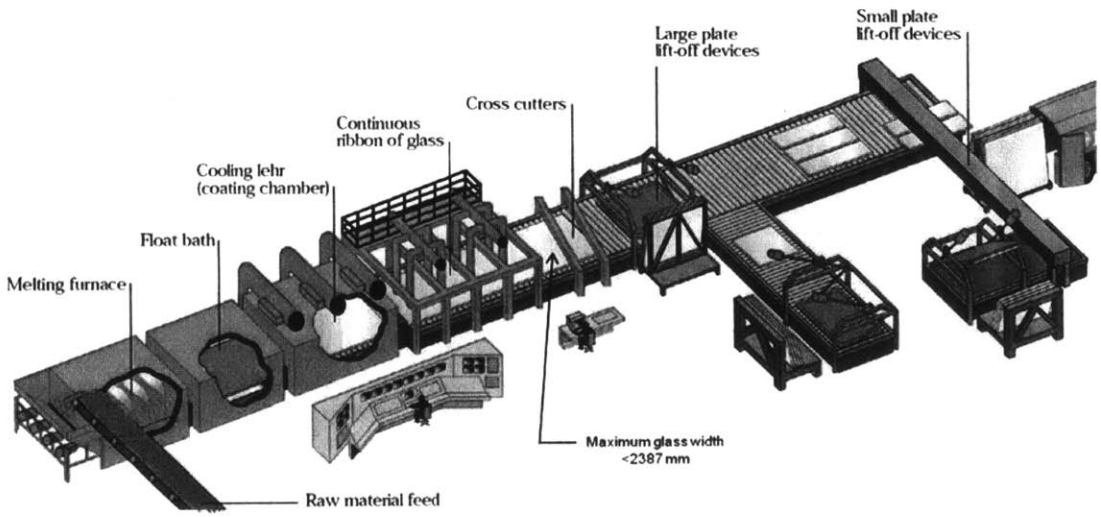

Figure 5: A diagram showing each step in the Float Glass manufacturing process. Image source: NSG Group

The demand for window panes increased throughout the late 19th century, which lead to the development of more efficient ways to manufacture flat sheets of glass. Initial attempts in manufacturing flat glass include Emile Foucault's vertical glass draw tower and the Pilkington Brother's (with Ford Motors) horizontal drawn twin-grinding process[37]. These techniques left defects on the glass and required large amounts of energy to polish[37].

In 1959 Pilkington Brothers came up with a process that fundamentally transformed the manufacturing output of glass: The Float Glass Process[37]. This process flows molten glass onto a liquid tin bath (Figure 5)[37]. Glass floats on top of the bath of tin, and eliminates the need for any energy intensive polishing processes[37]. The drawn glass sheet passes through an annealer to relieve internal stresses and is then cut down to the desired panel sizes[37].

The float glass process enabled glass to become a wide spread material with automotive windshields and façade glazing systems as its primary applications. This manufacturing process has fundamentally transformed architectural design during the 20th century with the ubiquitous implementation of the unitized glass curtain wall system on high-rise towers across the world.

1.1.3.2. LENSES

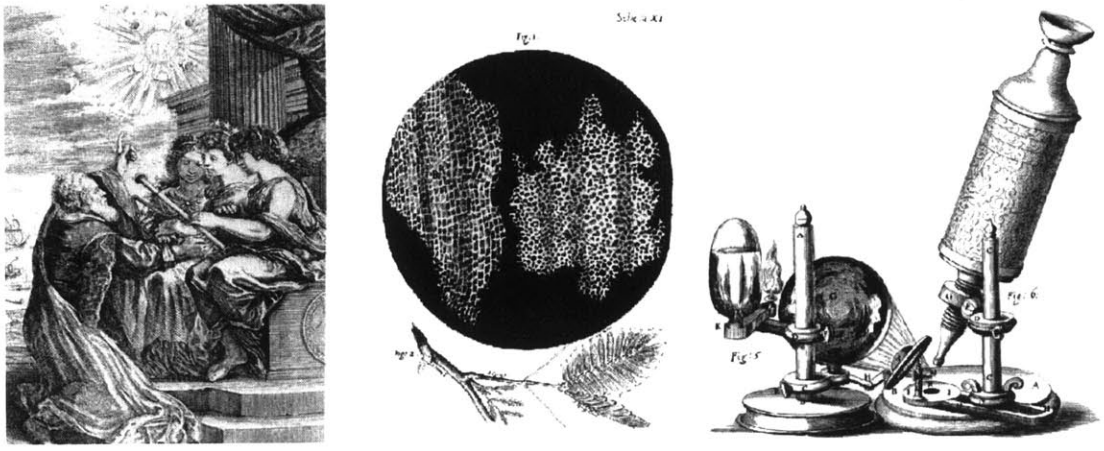

Figure 6: (A-left) Galileo Galilei using his telescope to study the sky. Image source: Lab Spaces (B-right) Robert Hooke discovering cells through his microscope. Image source: History of the Microscope

Glass' ability to manipulate light waves augmented human's capacity to see a new range of scales: from down into the petri dish to out in the vast depths of the universe. In the beginning of the 17th century lenses were invented, and Galileo Galilei developed a telescope, which he used to study the heavens (Figure 6A) [37]. Seeing into the depths of space, Galileo discovered the stars and geographical information about the moon[37].

In the late 17th century Antonj Van Leeuwenhoek was able to see spores by developing a microscope that had a spherical lens[37]. These technologies led to Robert Hooke's compound microscope, which he used to discover cells (Figure 6B) [37]. Hooke's microscope had three lenses: the first outer lens collected the light, the internal two created the magnification effect to see the formed image[37]

The new glasses in which humans had to see the world, drove technological developments in the field of optical lenses, through human desires to see deeper, farther and clearer. Most notable inventions were the following: Sir Isaac Newton's reflecting telescope which used mirrors to provide optical clarity, J. Franklin Hyde's process to create fused silica from igniting silicon tetrachloride gas / silicon rich gas, applied in the production of space shuttle windows and telescope mirrors, Augustin Fresnel's Fresnel lens technology that reflected and refracted light to create car and traffic headlights, to lighthouse lenses, and glass fibers used for optical communication systems across the world[37].

1.1.3.3. AUTOMATED GLASS FORMING

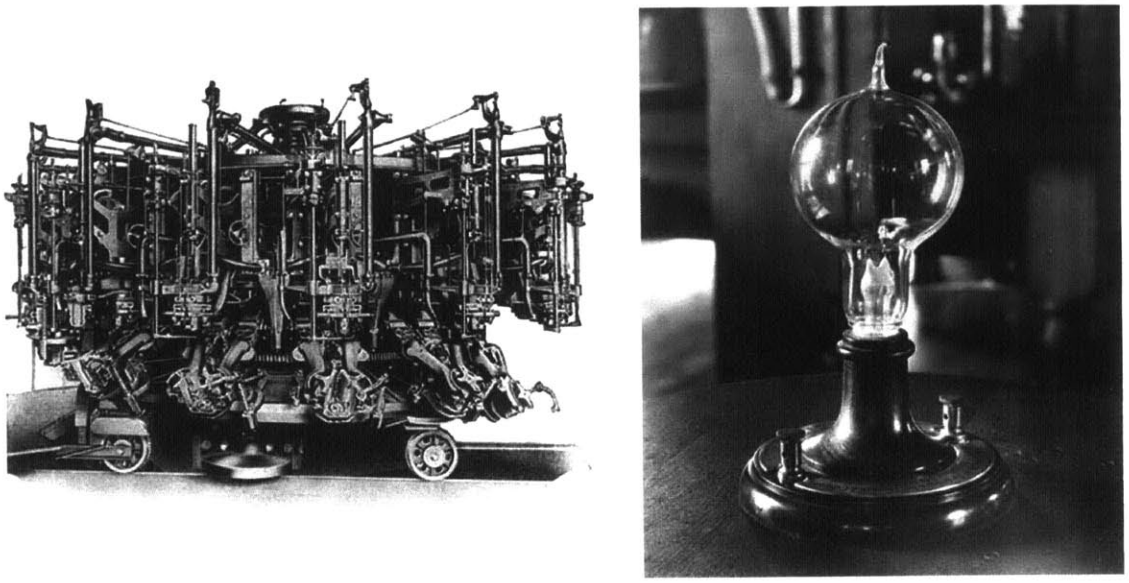

Figure 7: (A-left) A concept drawing of the Owens Bottle Machine. Image source: University of Houston (B-right) Thomas Edison's first light bulb. Image source: National Park Service

During the late 19th century, the industrial revolution brought automated processes into manufacturing pipelines through the rise of machines. The glass industry was one of the last domains to benefit from machine automation due to the levels of difficulty associated with handling the material[37].

Michael J. Owens received the patent in 1904, for the Owens Bottle Machine (Figure 7A), a manufacturing technology that could automate bottle making, rendering conventional labor-intensive techniques obsolete[37]. The American Society of Mechanical Engineers, proclaimed the technology as, "The most significant advance in glass production in over 2,000 years[37]." Owens proceeded to form Owens-Illinois Glass Company, which would turn out to be one of the most influential shapers of the glass industry we know today[37].

Thomas Edison developed the light bulb in 1879 (Figure 7B), and realized he needed a glass vessel to house his slow-burning filament[37]. The concurrent development of automated bottle machinery enabled gob forming techniques to be translated to the high-throughput manufacturing of glass light bulbs[37]. William Woods was the inventor who pioneered the technology in 1922: The Ribbon Machine[37]. The machine poured glass into a mold that output a ribbon of glass blanks, which was then met with blowing tips to inflate the bulbs[42]. To this date, the machine is one of the fastest manufacturing processes for such vessels[37].

While the integration of automated processes with glass forming techniques has enabled more efficient material processing and higher manufacturing speeds, what we are able to make with glass is tightly coupled with the way we make it. The reality is, the forming techniques humans use haven't evolved much since the ancient Egyptian era: we still blow, mold and cast glass.

However, the past few decades have seen a rise in complex fabricated products due to innovations in the field of Additive Manufacturing.

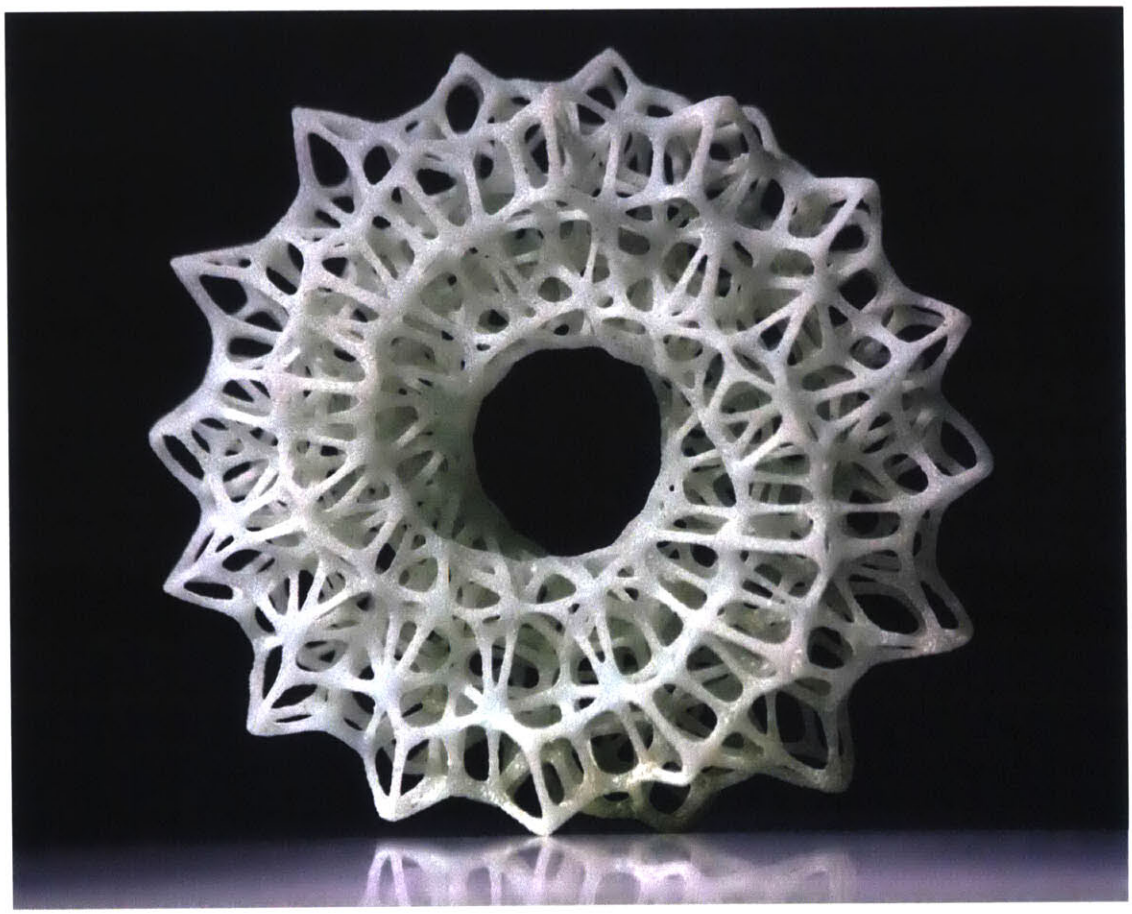

Figure 8: ExOne/Shapeway sintered glass via binder jetting process. Image source: Desktop Engineering

Additive Manufacturing (AM) has undergone significant developments since its conception as documented by Charles Hull in his patent of 1984 for the construction of parts using a photo-crosslinkable polymer[1]. Numerous processes have since been introduced, as summarized by the American Society for Testing and Materials (ASTM) which defined seven categories according to which the wide range of processes can be classified[2]. Each of the various approaches relies on different physical characteristics and phenomena, and is often associated with specific materials.

Throughout the history of manufacturing, the design process has often been guided by the constraints of the fabrication method. Current freeform fabrication capabilities enable a more flexible design space: fewer design constraints provide entirely new opportunities for the construction and assembly of objects at different length scales. Specifically, additional

complexity in product scale is now possible without negatively affecting its production rate, cost, or quality. Furthermore, AM allows for simple, rapid, and economic design iteration, capitalizing on the efficacy of non-linear design and optimization.

Extruded material built in three dimensions has proved its commercial value with the development of an entire consumer-level industry based on the principles of Fused Deposition Modeling (FDM)[3]. However, FDM printers, in their current embodiment, are unable to handle high melting point materials, and require feeding the material in filament form, thereby presenting significant limitations in size and scale[1].

Two 3D printing methods are typically used for higher melting point materials, such as metals and ceramics. The first one consists of a sintering method where particles are fused together below the melting point temperature. Parts are generally printed via binder jetting on a powder bed, where a binding agent temporarily joins particles until they are sintered through bulk thermal treatment[4] (Figure 8). The second method uses a laser (Selective Laser Melting, SLM) or another thermal source to melt material particles that are either injected or present on the building platform[5,6].

Glass-based materials hold the potential to provide particular value in the additive manufacturing field due to their hardness, optical qualities, affordability and availability. To date, binder jetting approaches have been applied to glass materials in order to overcome their high melting temperatures and high viscosity[4,7,8]. Sintered glass objects printed in this method are commercially available, but they are extremely fragile and appear opaque due to the light scattering from glass powders caused by incomplete densification (Figure 8) [9].

Robocasting has also been investigated for the manufacturing of glass components, with particular interest in Bioglass® formulations for bone tissue engineering. In this process, glass particles are suspended in an aqueous solution or incorporated into a binder matrix. The mixture is then extruded through a nozzle to form a porous green body. As the green body undergoes sintering however, it encounters the same limitations of the binder jetted glass parts described previously[10–12].

Moreover, even the most recent experiments with glass SLM have not been able to overcome such issues: products remain opaque and show poor mechanical properties. Furthermore, polishing requires extensive effort, access to all geometry and often results in the samples breaking into smaller pieces. Even when successful, internal porosity leads to significant light scattering, thus limiting transparency when implementing this method[13]. A

manual wire feeding approach described in the same work yielded higher quality results; however, lack of automation limits control and prohibits part production.

The extrusion of molten glass remained in traditional glass manufacturing practices. In fact it is still applied in the artistic milieu: commercial kiln packages such as Bullseye Glass Co.'s Vitrigraph, enable glass artisans to create glass canes or stringers through manual glass extrusion, ranging in diameter from fractions of a millimeter to several millimeters[14].

Large scale manufacturing processes have also been developed for glass extrusion; they are particularly suitable for glass characterized by a narrow working range and a very high softening point; such as silica glass (softening point ~1600°C) or with a strong tendency to crystallize such as borosilicates. The application of pressure to force glass flow through a dye extends the glass working range to higher viscosities, and enables the production of rods and tubes with complex sections[15].

The following chapters will present the development of tools and processes, which culminated in the first of its kind *fully functional material extrusion system for optically transparent glass,* along with initial explorations in glass sintering. This enabling technology and related platform is comprised of scalable modular elements able to operate at the high temperatures required to process glass from the molten state to the final annealed product. Automated extrusion of 10 mm diameter glass beads with a build rate of about 460 mm^3/s enabled the creation of 3D parts as described by Computer Aided Design (CAD) models with a build volume of 250 mm x 250 mm x 300 mm.

The additive manufacturing system and printed parts provide proof-of-concept for automated glass deposition and the ability to produce objects within an expansive design space. This method enables production of parts that are highly repeatable, allow light transmission, and resemble glass as conventionally produced. Printed components can be modular and scalable from artistic products to architectural constructions, as it can be seen by the examples included herein.

Chapter 2

METHOD A: GLASS SINTERING

The Lichtenberg and Direct Spark Sintering technique that is discussed in *Method A: Sintering Glass* has been developed by Steven Keating, PhD Candidate from the Mediated Matter Group. All work presented in the following chapter has explored techniques from Steven's research.

Contributors: Steven Keating, John Klein, Benjamin Jennett, James Weaver, Prof. Neri Oxman

METHOD A: GLASS SINTERING

2.1. DIRECT SPARK SINTERING

Figure 9: Varying glass compositions collected to experiment with additive sintering processes: Soda-lime glass #13-104 grits, recycled soda-lime glass, borosilicate, boromax frits, Moroccan sand, quikrete aggregate, black sand, magnetite sand, lunar and martian regolith

While numerous approaches exist to utilize heat to solidify glass, the research explored three sintering techniques with potential for ease of automation and form generation. These methods include 1) direct spark sintering, 2) a novel process termed Lichtenberg Sintering (by Steven Keating) that was inspired by the fractal geometry inherent to the technique and 3) Selective Laser Sintering. A range of glass samples were collected to explore the sintering processes ranging from soda ash glass, glass boromax frit, glass beads fine-coarse and varying compositions of raw sand (Figure 9).

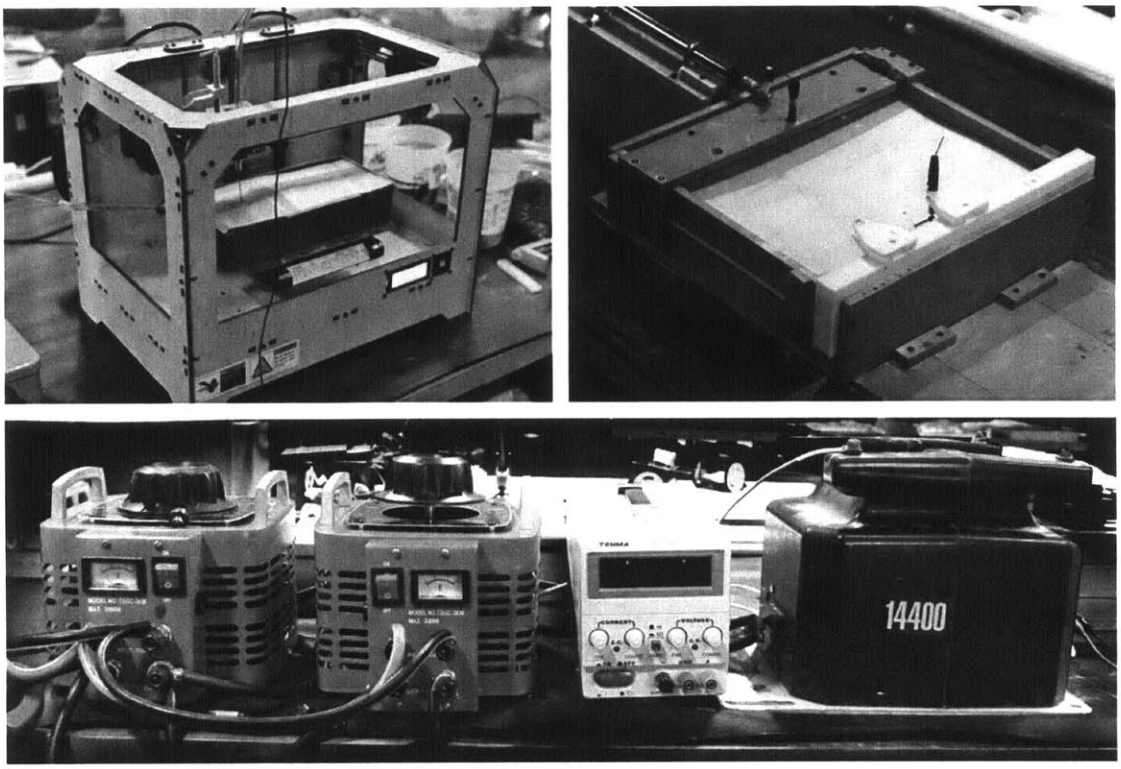

Figure 10: (A-top right) Test bed high voltage setup (B-top left) Modified makerbot replicator 2 for sintering (C-bottom) Single axis drive rail setup to sinter mechanical testing samples

Through initial experiments, the direct spark electrosintering fabrication approach has demonstrated a capacity to sinter the granular materials (35-88 micron soda ash glass powder) rapidly using high voltages and power in excess of 1 kW. The test bed high voltage setup is comprised of a 220V 60A variable autotransformer and a 14,400V line transformer (Figure 10A). There are two different methods to form members using electro-sintering: the one electrode drag (1ED) and the two electrode drag (2ED) techniques. The 1ED and 2ED setups were tested on a modified makerbot replicator 2 (Figure 10B) and on a single axis rail driven with a low voltage linear actuator (Figure 10C).

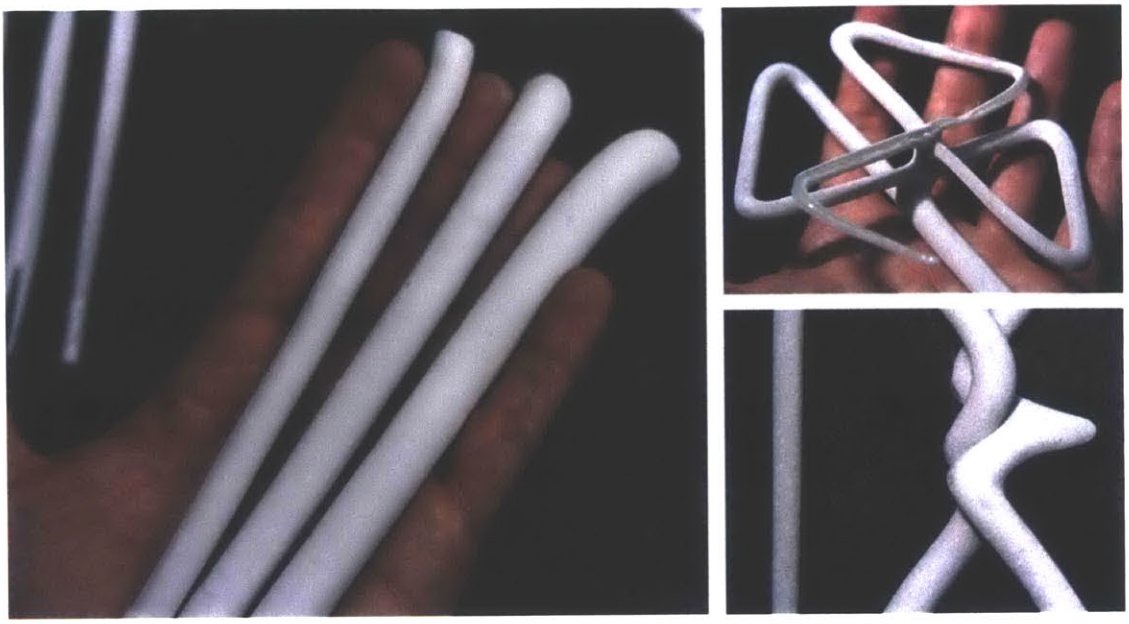

Figure 11: (A-left) Electrosintering experiments using direct spark sintering allows for designed structural members to be formed additively with controlled geometries (B-top right) Path bridging effect (C-bottom right) Member resolution and material build up

The 1ED leaves the first electrode static while dragging the second electrode through the granular mixture. This maintains a live current running through the drag path and continually increases the thickness of the member due to the dissipation of heat. Large member elements have been produced with a rod diameter of around 0.75" (Figure 11A). The 2ED method pulls the two electrodes through the granular mixture together, which sinters the material between the two electrodes in a more controlled manner. (Figure 11B) shows a path bridging effect that occurs when the print path overlaps on itself, causing the electricity to find the minimal path of least resistance. This technique led to the design of overlapping print paths that created lattice like structures from the bridging effect. (Figure 11C) shows the resolution of a connection detail from a sintered component, and the heat buildup, which occurs from acute path angles.

2.2. LICHTENBERG SINTERING

Figure 12: (A-bottom) Lichtenberg sintering electrode setup (B-top) Sintered glass Lichtenberg structure (Image credits: Steven Keating)

The Lichtenberg Sintering technique is a process that sinters glass along fractal paths, and generates a diffusion-limited aggregation type of structure. Similar to the Lichtenberg structures (fulgurites) formed through natural lightning strikes on silica-based soils, the process develops optimal fractal geometries through the fabrication process itself. Two electrodes are placed separately inside a granular bath with a small amount of conductive media to facilitate a starting current flow (Figure 12A). In these experiments, glass powder is the granular media and a small amount of dispersed water provides the initial conductive path. As the current flows, glass particles become heated along main current paths and the structure progresses due to increased conductivity in heated glass. The water evaporates from the heat and the current flows through the heated glass, sintering the powder together in fractal structures optimized by the dielectric breakdown process physics. The fabrication process time is controlled by the current flow and handheld samples in our setup were constructed in seconds.

The Lichtenberg fractal structure (Figure 12B) is similar in morphology to fractals found in natural systems, such as rivers deltas and biological vein networks. The exploration from this work holds potentials for its natural branching system.

Preliminary design attempts were made to control the overall geometries through different ceramic molds and varying compositions of glass. The small soda-lime glass grits had the most successful results, and glass fusion details can be seen in the SEM images, which reveal a high bondage occurring at the core of each fractal as a result of a higher heat concentration (Figure 13).

Figure 13: SEM of the Lichtenberg glass fusion details (Image credits: James C. Weaver)

2.3. LASER SINTERING

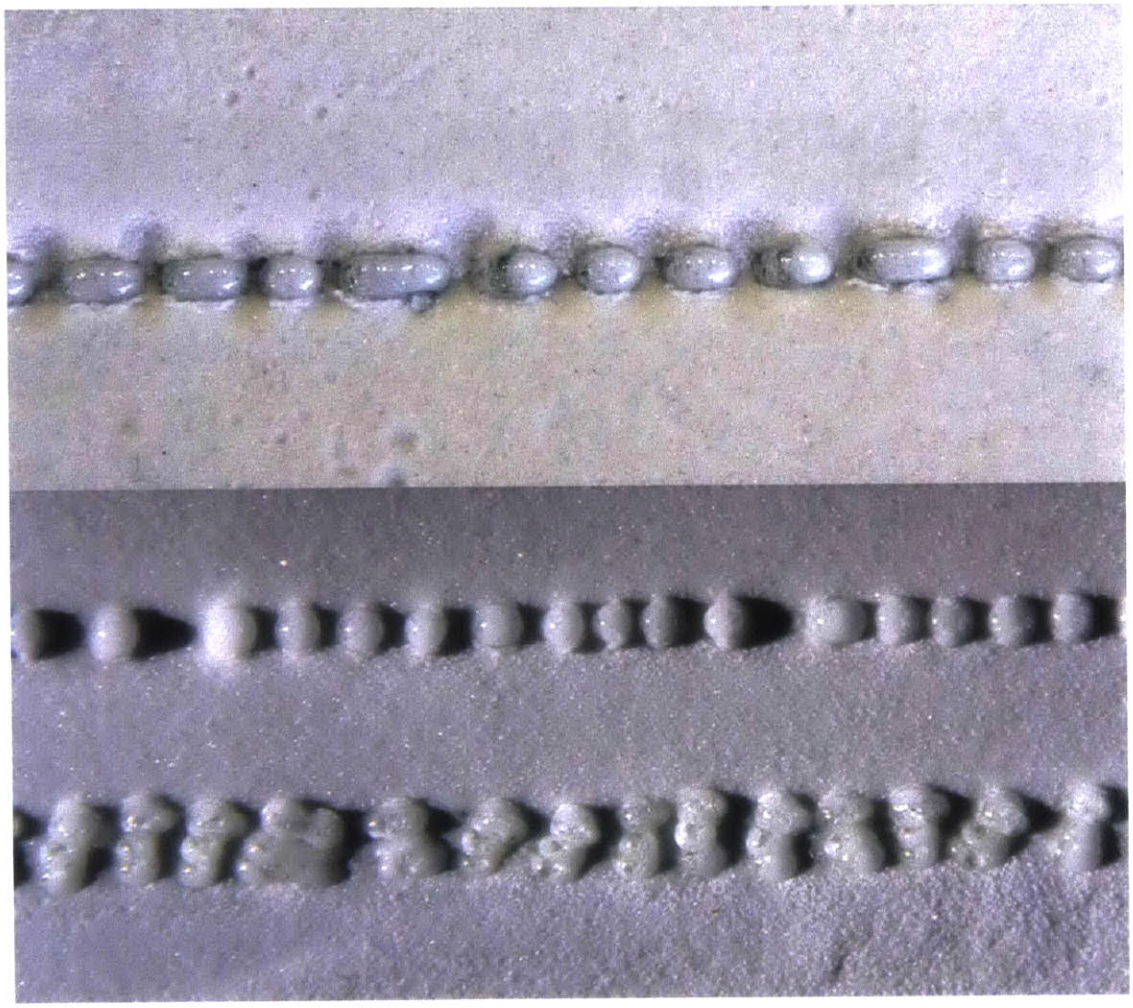

Figure 14: (A-top) Melted glass clustering into droplets (B-bottom) Bonding occurring in the Z axis and not the X & Y

In a preliminary attempt to reduce the amount of energy required to melt the 35-88 micron soda ash glass powder, a Selective Laser Sintering (SLS) approach was pursued by modifying a Universal PLS6.150D 150w laser cutter. A MDF container was built with an attached powder hopper to deposit a layer of glass powder after each fused layer was complete. The initial tests proved to be successful in melting the glass powder; however, preventing the melted glass from clustering into droplets was rather challenging (Figure 14A). The droplet formation prevented layer bonding in the X & Y axis resulting in unsuccessful parts. Bonding in the Z axis proved to be successful and was a byproduct of the thickness of the newly deposited glass

layers (Figure 14B). Additionally, the settings that were needed to melt the glass were not sustainable for long duration runs of the laser cutter, and further attempts should be explored on a higher power setup.

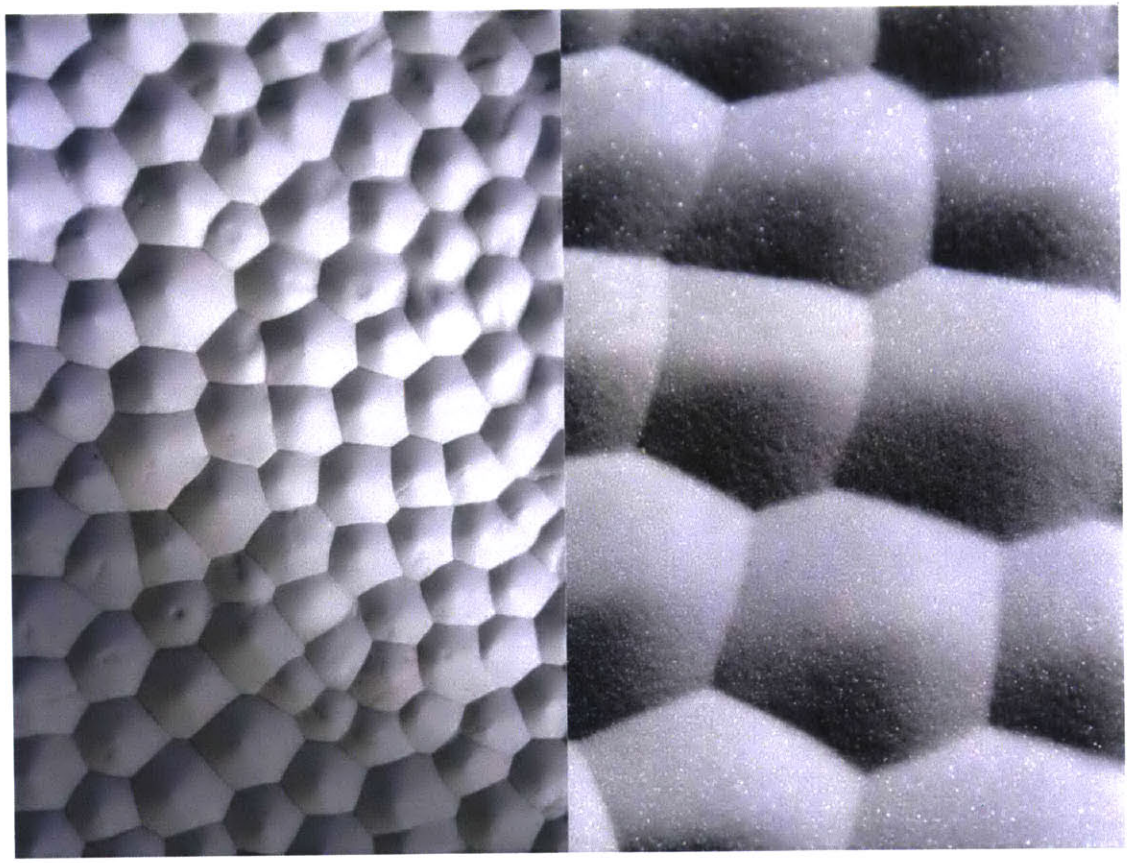

Figure 15: An unsuccessful attempt to melt Deposited glass powder into 3D objects

After experiencing difficulties with the X & Y layer bondage, a different approach was tested where the glass powder was locally deposited (Figure 15), then melted in order to achieve better fusion. The pyramid buildup of the glass powder made it even more difficult to melt consistently, and this approach was considered unsuccessful.

While all the sintered glass approaches proved to be successful in their capacity to sinter glass particles, the optical qualities of the glass were distorted from the light scattering of the <100micron soda-ash glass beads, which did not encounter complete densification. This directed the research to pursue a different approach to achieve optical clarity from glass: Fused Deposition Modelling (FDM) starting from molten glass.

Chapter 3

METHOD B: GLASS FDM

The research that is discussed in *Method B: Glass FDM* was developed as part of collaboration between the MIT Media Lab's Mediated Matter Group and the MIT Department of Material Science and Engineering's Glass Laboratory. This chapter is adapted from a journal article; *Glass 3D Printing*, which will be submitted to the *3D Printing and Additive Manufacturing Journal*.

Authors: John Klein, Michael Stern, Giorgia Franchin, Markus Kayser, Chikara Inamura, Shreya Dave, James C. Weaver, Peter Houk, Paolo Colombo, Maria Yang and Neri Oxman

3

METHOD B: GLASS FDM

3.1. SYSTEM DESIGN AND CONSTRUCTION

3.1.1. SYSTEM IMPLEMENTATION

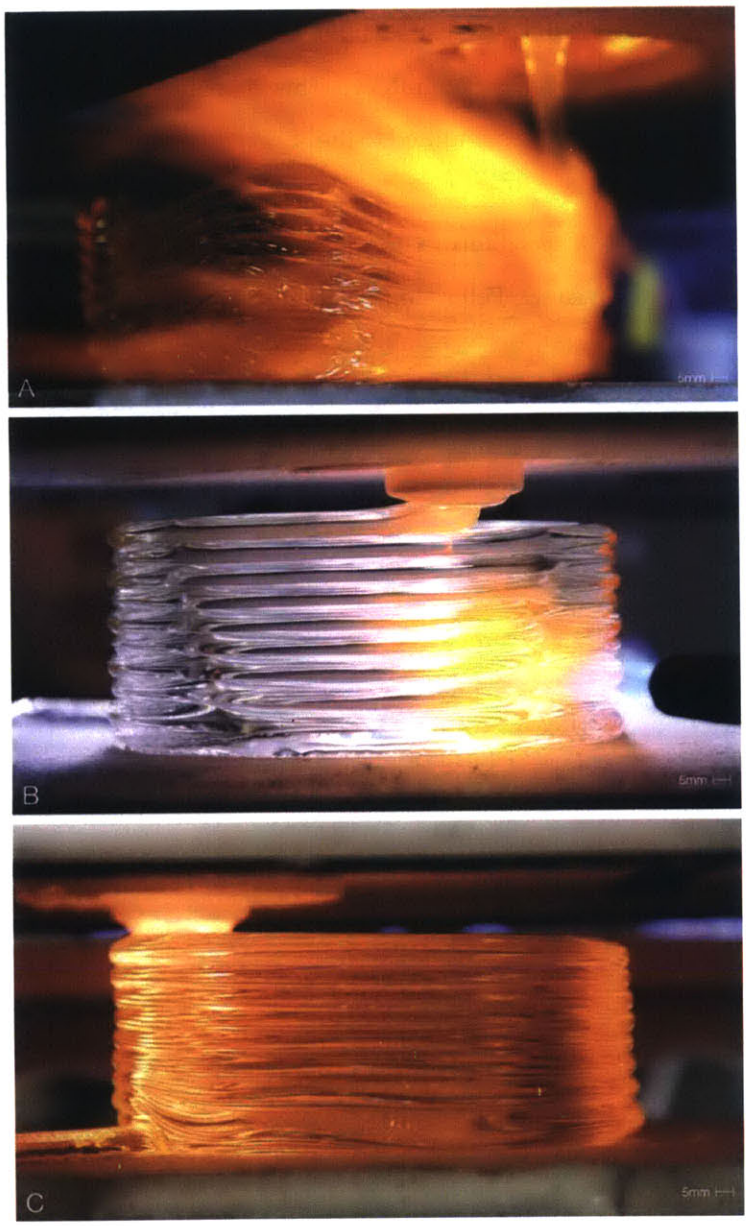

Figure 16: Evolution of the printing process from its early stages (A) Printing in ambient air with no nozzle (B), printing in ambient air with a nozzle (C) the current setup with an annealing chamber

The apparatus design and construction was guided by a series of successive tests with increasing complexity and control. They served as demonstration of operation of the printer and are briefly presented below to illustrate the evolution (Table 2).

Table 1. Glass 3D Printer evolution steps.

1	Gravity feed proof of concept
2	Kiln auto-coiling, fixed Z
3	Kiln auto-coiling, moving Z
4	Kiln manual XY control
5	Kiln automatic control
6	Nozzle
7	Annealing chamber

Initial tests were conducted using a previously heated ceramic crucible; molten glass was added and a slow flow was observed through the hole at the base. The tests proved that gravity-driven feed was feasible, but suggested that heating of the feed material would be critical. The second step involved the addition of a kiln surrounding the crucible during the process; glass flow of continually heated feed material was demonstrated. Flow was continuous and the glass was allowed to coil autonomously, forming tapered cylindrical shapes.

Computer control of the Z-axis was then implemented which enabled the system to maintain constant deposition height and to produce coiled cylinders with constant diameters. To create the first designed shape, bumpers were mounted on the frame and the crucible kiln was manually moved, successfully producing a square cross-section object. Digital control on the X and Y axes was then added, and more complex shapes were successfully fabricated. Implementation of software and motion control also provided the chance to set a constant travel speed. A rectangular prism being printed with this setup is presented in (Figure 16A).

Despite the motion system reaching satisfactory mechanical control and precision, the printed parts showed inconsistent filament diameter, poor adhesion between layers and rapid accumulation of defects. These problems derived from a common cause: the fact that glass was dripped from an offset height. An independently heated ceramic nozzle to be attached to the crucible was therefore designed and produced; with the nozzle tip was below the carriage level it was possible to print with no offset height. With this upgrade, control of the layer height was

achieved and the above-mentioned issues were overcome. A cylinder being printed after the addition of the nozzle is shown in (Figure 16B).

Glass objects need to be cooled down to room temperature in a slow and controlled way through the glass transition temperature range, the annealing process, to release permanent stresses associated with thermal gradients that otherwise would lead to the spontaneous breakage upon cooling. The 3D printed parts were kept above the annealing temperature (Ta) with the help of propane torches (visible in Figure 16A-B) and were annealed right after the printing completion; the torching process was not automated and difficult to control, and therefore often the objects cracked. Finally, the introduction of a heated build chamber enabled in situ temperature control. (Figure 16C) shows the same build as in (Figure 16B), this time being printed directly into the heated build chamber providing consistent annealing temperature and eliminating the need for torches. The final setup resulted in a fully automated process and the capability to produce larger and stronger parts.

3.1.2. HARDWARE

3.1.2.1. HEATING ELEMENTS

The primary components of the system were the Kiln Cartridge (which contains a Crucible Kiln and Nozzle Kiln) and the Print Annealer (heated build chamber). A schematic of the whole assembly is shown in (Figure 17A).

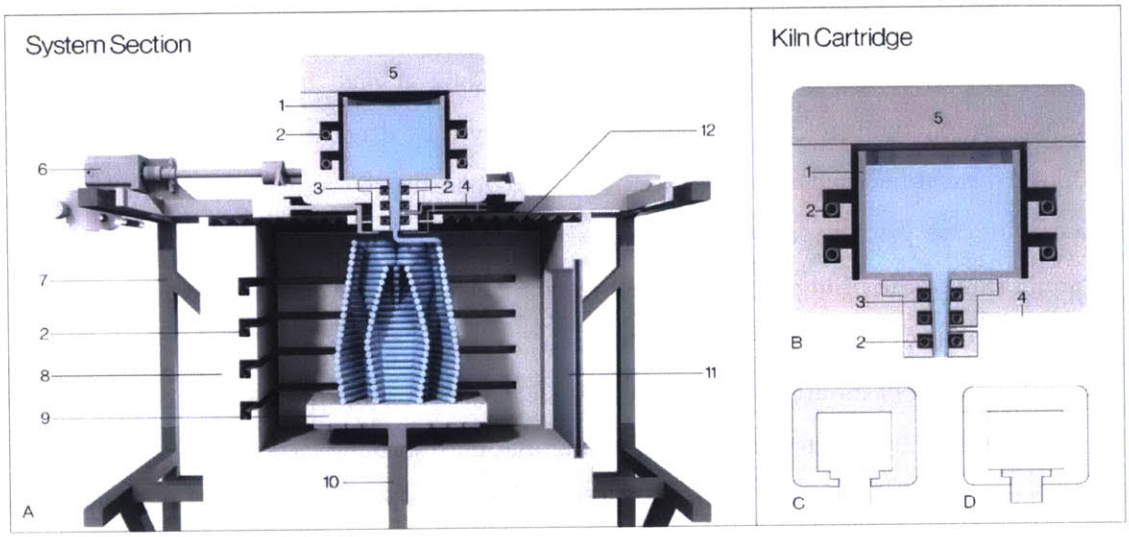

Figure 17. Rendered cross-section of the system showing (A) the printer during fabrication, (B) the Kiln Cartridge C) the Crucible Kiln and (D) the Nozzle Kiln. Detail elements are as follows: (1) the crucible, (2) heating elements, (3) the nozzle and (4) the thermocouple, (5) removable feed access lid (6) stepper motors (7) printer frame (8) Print Annealer (9) ceramic print plate (10) z-drive train (11) ceramic viewing window (12) insulating skirt

Inside the Kiln Cartridge (Figure 17B), the Crucible Kiln (Figure 17C) was an 1800W high temperature furnace that was used to melt and maintain molten glass at a temperature of 1040-1165°C. The kiln was made of alumina-silica fiberboard and it was heated through a FeCrAl coiled wire. Temperature was monitored via a Type K thermocouple.

The Nozzle Kiln (Figure 17D) was mounted to the bottom plate of the Crucible Kiln and provided 300W of heat to the printer nozzle. The kiln was constructed similarly to the Crucible Kiln (Figure 18A). Temperature was monitored via a Type S thermocouple for faster response times. Each component of the system was a modular unit, to allow quick development. All heating elements and thermocouples exited out to a single area in the Kiln Cartridge, reducing limitations on the printer movements.

Glass was contained in a refractory crucible placed inside the Crucible Kiln; the Nozzle Kiln provided control over the flow of glass. The crucible included a bottom hole where the

nozzle was inserted; the assembly was then sealed with a refractory mortar. The nozzle was machined from bulk high temperature alumina bisque ceramic rods (Figure 18B). The small dimensions of the nozzle allowed it to protrude below the carriage into the annealing chamber and enabled the direct deposition of glass with a precise control on layer height.

The glass was printed directly into the Print Annealer, which maintained a temperature above the glass transition temperature 480-515°C (Figure 19). The Print Annealer remained stationary while the Z-platform moved inside it. The Z-platform was fabricated out of a ceramic kiln shelf that enabled good initial bonding at high temperature and release at annealing temperature. The X-Y control was achieved by driving the print head. The 3300W Print Annealer had two alumina-silica fiberboard doors to provide access to the nozzle and for removing the printed part, and a transparent ceramic (Neoceram®) window that enabled monitoring of the print job. The annealing chamber was based on the GlazeTech kiln (Skutt Kilns, Portland, OR, USA).

The sealing of the annealing chamber was achieved through the addition of two light and thin alumina-silica fiberboard skirts assuring that the annealing chamber was always closed on the top. One skirt was mounted on top of the annealing chamber, and the other to the moving carriage below the feed kiln.

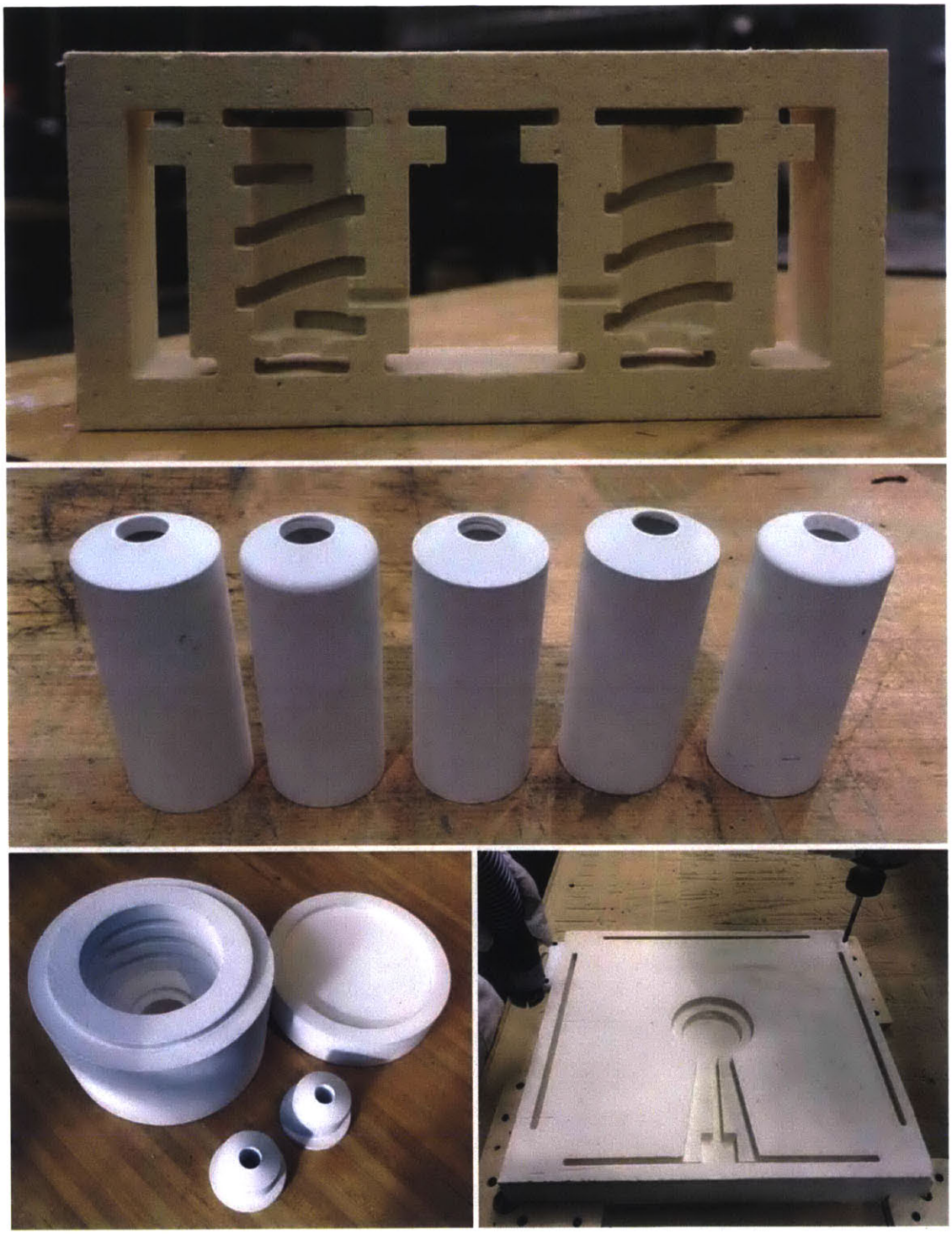

Figure 18: (A-bottom) The Crucible Kiln and Nozzle Kiln fabricated from alumina-silica fiber board (B-middle) Nozzles machined out of high temperature alumina bisque ceramic rods (C-top) Nozzle Kilns clam-shell fabrication strategy

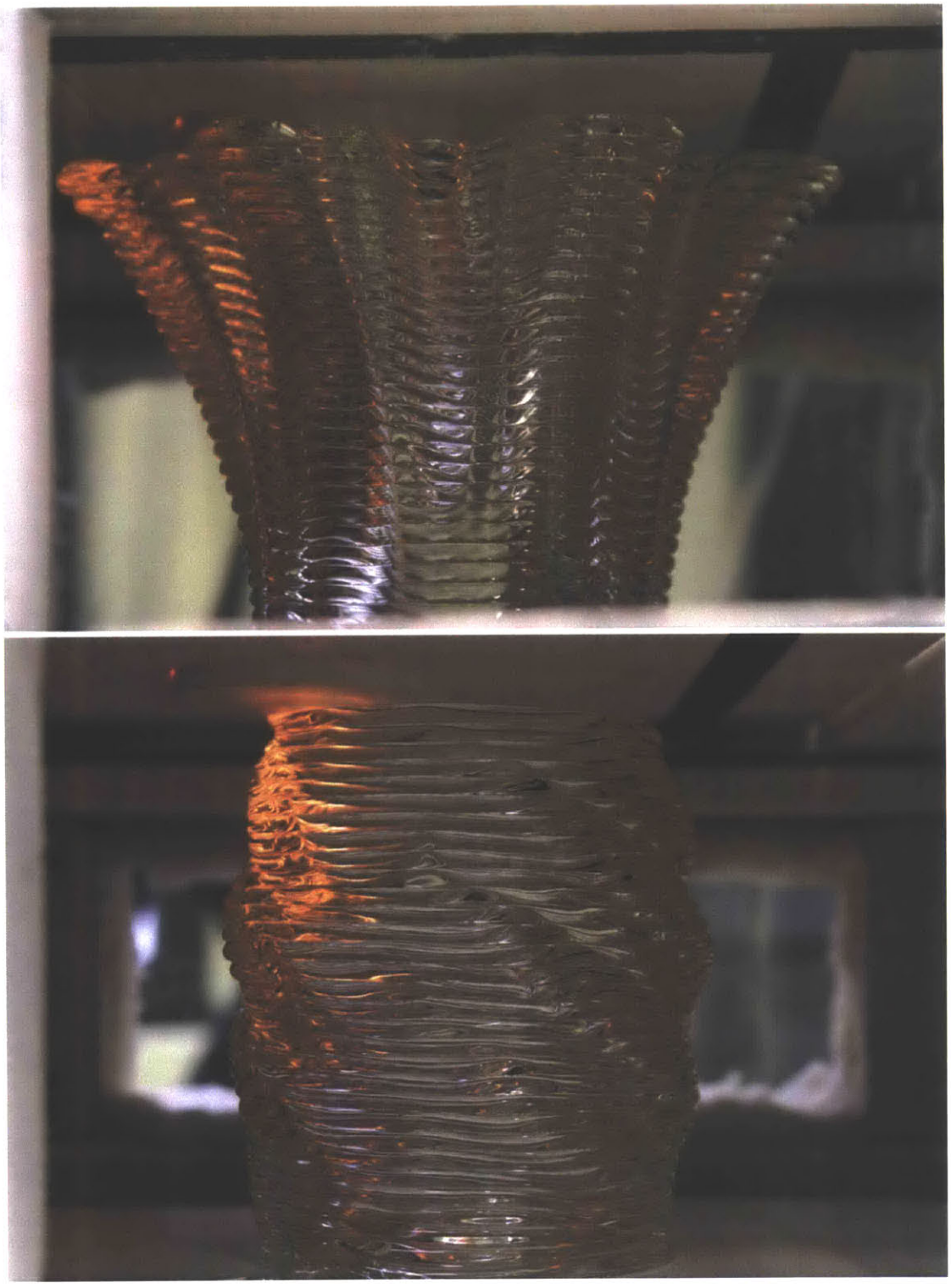

Figure 19: Depositing molten glass into the Print Annealer. The Print Annealer remained stationary while the Z-platform moved inside it. The Z-platform was fabricated out of a ceramic kiln shelf that enabled good initial bonding at high temperature and release at annealing temperature. The Nozzle Kiln and Nozzle can be seen in the top of both images

3.1.2.2. FRAME AND CARRIAGE

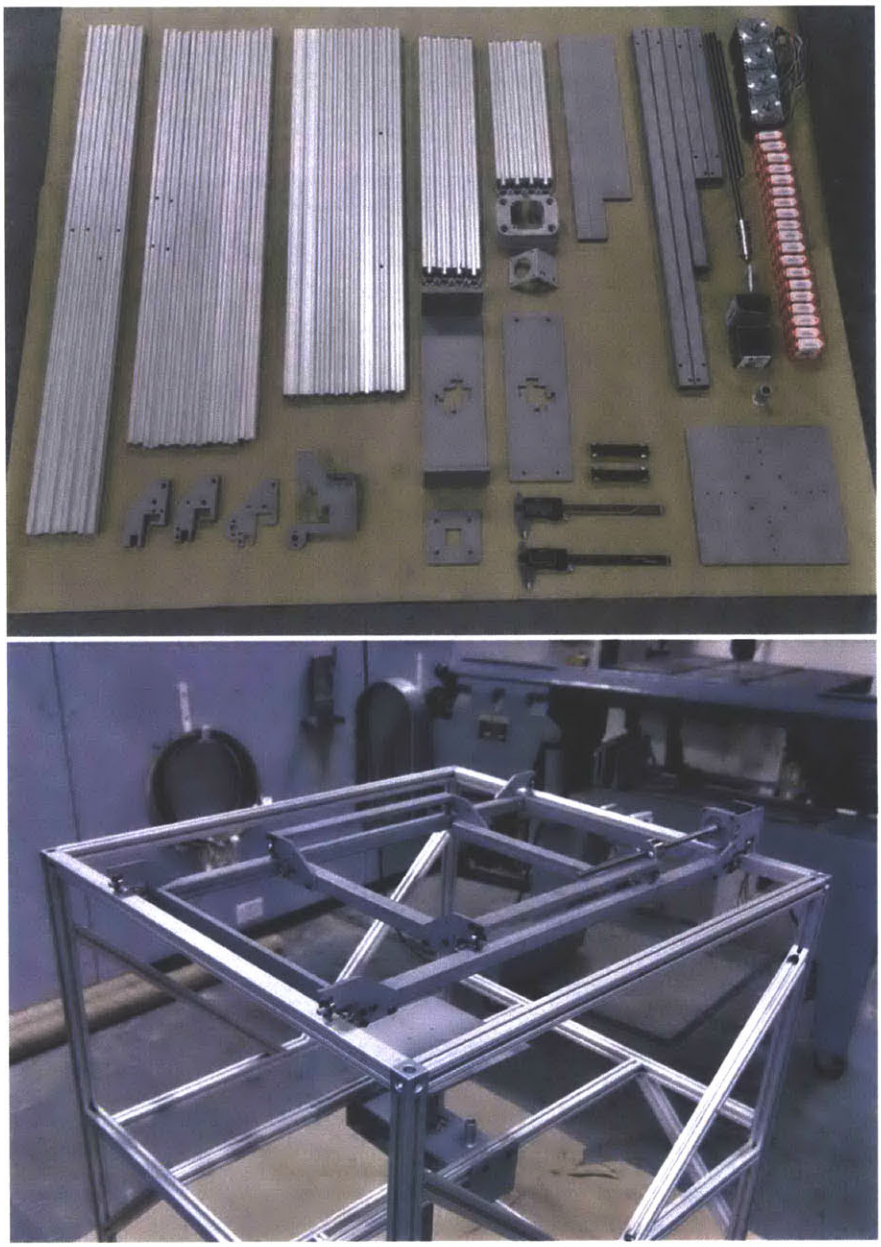

Figure 20: The assembled printer frame & carriage built in the Center for Bits and Atoms

The printer was constructed of 80/20 aluminum stock and square steel tube (Figure 20). Aluminum was used for components not exposed to high heat, while the heavier steel was reserved for central components that may become hot from the Crucible Kiln, Print Annealer,

or radiating molten glass. The Crucible Kiln carriage consisted of steel supports mounted on bearings that travelled on the structural steel tracks. The entire system was mobile, mounted on pneumatic casters to enable transportation without damaging the fragile ceramic kilns.

3.1.2.3. MOTORS AND BEARING BLOCKS

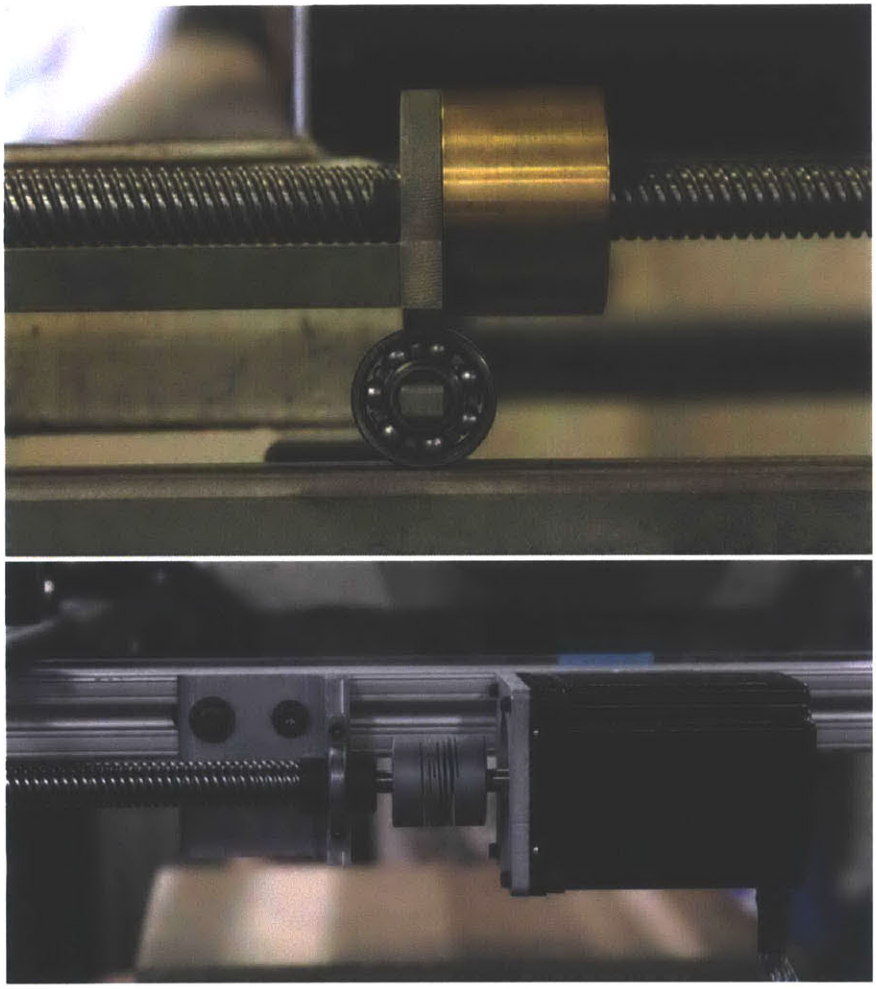

Figure 21: Stepper motor connected to ACME lead screws with flex. helical coupling

XYZ motion was provided by three independent stepper motors – lead screw gantry systems and drivers that were electronically controlled by an Arduino and a RAMPS 1.4 Arduino shield. The motors had a rated holding torque of 280 N·cm; the high-torque was required due to the inertia of the Kiln Cartridge and carriage assembly.

The motors were connected to ACME lead screws with flexible helical couplings to accommodate misalignments (Figure 21). The motors were isolated from axial and radial loads by bearing blocks. The Z motor was mounted at the base of the frame requiring only one hole at the base of the Print Annealer to accommodate the build platform support rod. Limit switches were mounted at the "zeros" of the X, Y and Z axes both to provide homing information to the control software and to protect the system from mechanical crashes. These prevented the motor from driving when activated and were connected directly to the RAMPS board. The limit switch cables were bundled separately from the motor cables to prevent interference.

3.1.2.4. SAFETY MEASURE

An emergency stop button (Figure 22), mounted to the frame for easy access, is wired to cut power to the drivers and motors. Limit switches are mounted at the "zeros" of the X, Y and Z axes both to provide homing information to the control software and to protect the system from mechanical crashes. These prevent the motor from driving when activated and are connected directly to the Arduino Shield. The limit switch cables are bundled separately from the motor cables to prevent interference.

Figure 22: Emergency stop button

3.1.3. SOFTWARE

3.1.3.1. CAD MODEL

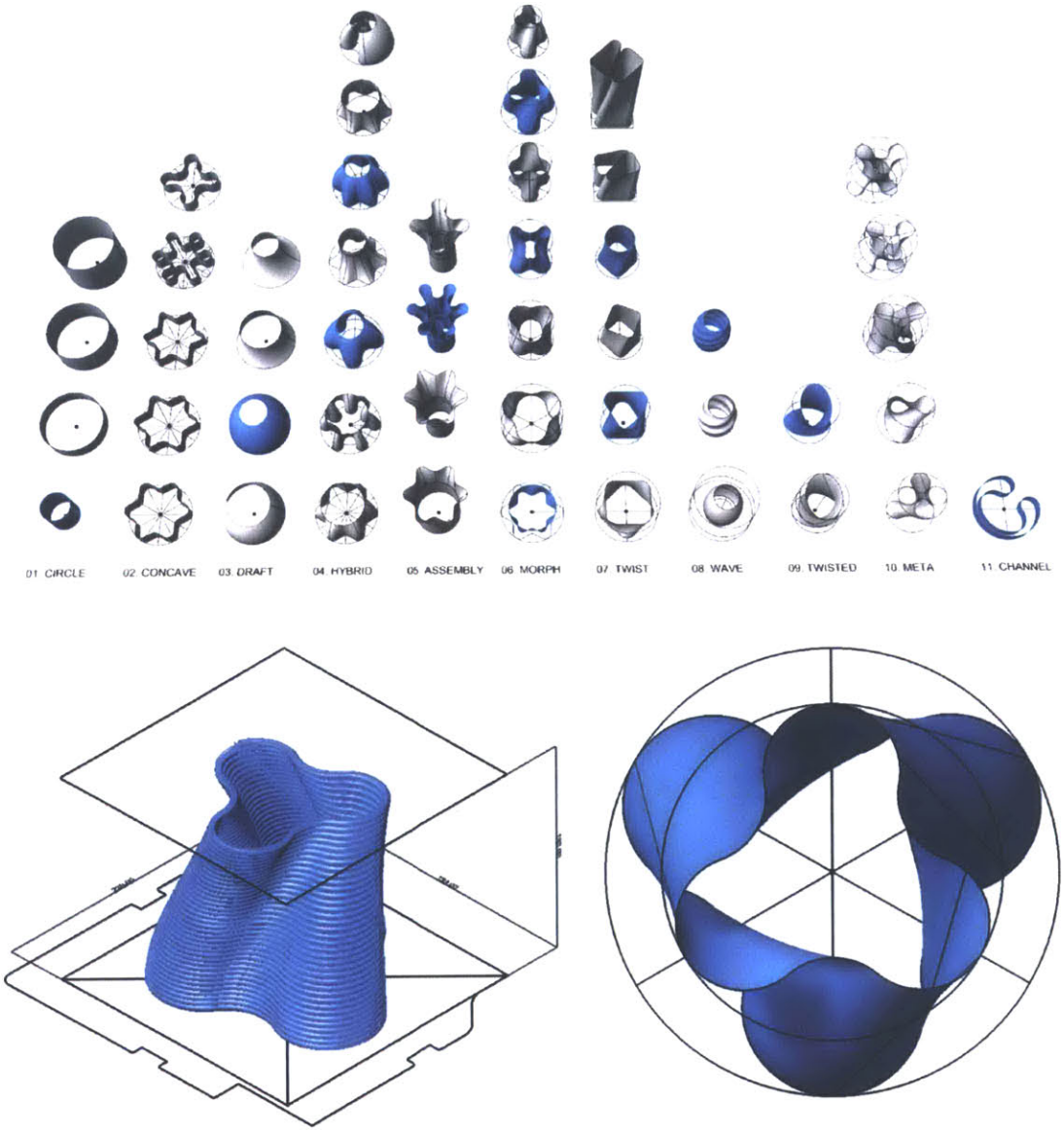

Figure 23: (Top) 3D design space (Bottom) 3D nurbs surface contained within the glass printer build envelope (250mm x 250mm x 300mm)

The 3D object was defined in Rhinoceros 5.0 environment. The model had to fit within the build chamber, i.e. 250mm x 250mm x 300mm (Figure 23). The input surface was described as a non-uniform rational basis spline (nurbs) geometry.

3.1.3.2. SLICING AND GENERATING G-CODE

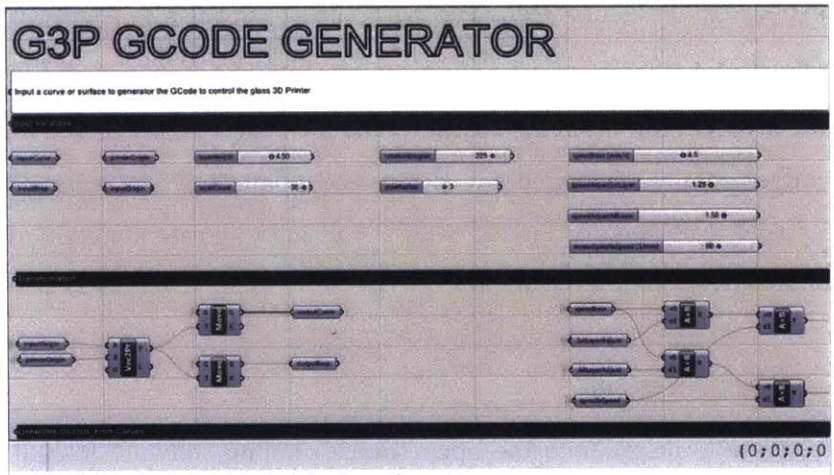


```
0 ; G3P g-code generated by Grasshopper
1 G21 ; set units to millimeters
2 G90 ; use absolute coordinates
3 ; Home xyZ
4 G1 X10 Y250 Z0 F270.000
5 ;copy g-code from GH here
6 G1 X221.591963937676 Y150.882277759791 Z0.0225000000002912 F337.5
7 G1 X220.722109263911 Y153.704401258509 Z0.045000000000245
8 G1 X219.646692055969 Y156.454766535481 Z0.06750000000022
9 G1 X218.371304941208 Y159.118294040156 Z0.0900000000002014
10 G1 X216.902867059127 Y161.680457737094 Z0.112500000000184
11 G1 X215.249465327399 Y164.127336637542 Z0.135000000000167
12 G1 X213.420116119645 Y166.445614213995 Z0.157500000000151
13 G1 X211.424949507496 Y168.622806477761 Z0.180000000000136
14 G1 X209.274555453675 Y170.646800415383 Z0.202500000000122
15 G1 X206.980847127397 Y172.506799834082 Z0.225000000000109
16 G1 X204.556148094855 Y174.192435333871 Z0.247500000000097
17 G1 X202.013793147053 Y175.694708584393 Z0.270000000000086
18 G1 X199.367617220172 Y177.005415709144 Z0.292500000000075
19 G1 X196.631945611073 Y178.117224501418 Z0.315000000000066
20 G1 X193.821745336539 Y179.024175441389 Z0.337500000000058
21 G1 X190.952274806898 Y179.721120708356 Z0.360000000000051
22 G1 X188.039296267922 Y180.204759781225 Z0.382500000000045
23 G1 X185.098616616344 Y180.47212817829 Z0.40500000000004
24 G1 X182.146265014582 Y180.521696253991 Z0.427500000000037
25 G1 X179.198344888729 Y180.353341281416 Z0.450000000000034
26 G1 X176.270897740127 Y179.968167464651 Z0.472500000000032
27 G1 X173.379840777899 Y179.368319007184 Z0.495000000000032
28 G1 X170.541015021386 Y178.556652483182 Z0.517500000000032
29 G1 X167.769475946235 Y177.538970012114 Z0.540000000000033
```

Figure 24: G3P custom GCODE Generator. User inputs surface to create GCODE

The surface was sliced using a custom C# script in Grasshopper Build 0.9.76.0 (Figure 24). The slicing script drew a helix around the CAD model structure, enabling continuous flow and accommodating for the specific filament diameter of extruded glass. This toolpath was then represented in Cartesian coordinates in the form of G-code. The layer height, curve discretization, and feed rate, could be modified in real-time, while the tool path could be monitored in the preview pane. Users could also define specific velocities for each point. The algorithm developed for the wrapping toolpath started from the input surface, intersected it based on the layer height, discretized each intersection curve based on the input resolution, and then incrementally remapped the discretized points with increasing Z values. The remapped points were then connected with a polyline to create the continuous wrapping toolpath for any given complex geometry.

3.1.3.3. MOTION CONTROL

G-code files were imported into the open source printing software Repetier-Host V1.0.6. Repetier firmware, adapted for the acceleration, velocities, and size of the build platform, was used to direct the printer.

3.2. SYSTEM OPERATION CHARACTERIZATION

3.2.1. MATERIAL CHARACTERIZATION

Commercial soda-lime glass nuggets (System 96® Studio NuggetsTM, Spectrum® Glass Company, Inc., Woodinville, WA, USA) were used in this study.

Glass density and thermal expansion coefficients (CTE) at low ($T \leq 210°C$) and high ($T = 1000°C$) temperature were estimated based on the glass composition. Fluegel models16,17 were applied. Data are provided in (Table 3).

Table 2. System 96® Studio Nuggets™ density and CTE estimations at different temperatures

Density & CTE	
T_0 (°C)	20
ϱ_0 (g/cm^3)	2.53
T_1 (°C)	210
CTE_1 (x10^{-6} K^{-1})	9.8
T_2 (°C)	1000
ϱ_2 (g/cm^3)	2.34
CTE_2 (x10^{-6} K^{-1})	32

Glass dynamic viscosity η strongly depends on temperature; its dependence can be modeled using the so called Vogel-Fulcher-Tammann (VFT) equation: 18–20

$$\log\eta(T) = A + \frac{B}{T - T_0} \quad (1)$$

where η [Pa·s] is the dynamic viscosity of the glass, T [°C] is its temperature, and A, B and T0 are experimental values depending on the glass composition.

Viscosity values were measured at different temperatures at Corning Inc. (Corning, NY, USA) with proprietary equipment. Experimental data were fitted using the VFT equation to estimate A, B and T0, leading to the results shown in (Figure 25). The VTF equation enables prediction of glass viscosity at each temperature, thus allowing flow estimation and process tailoring.

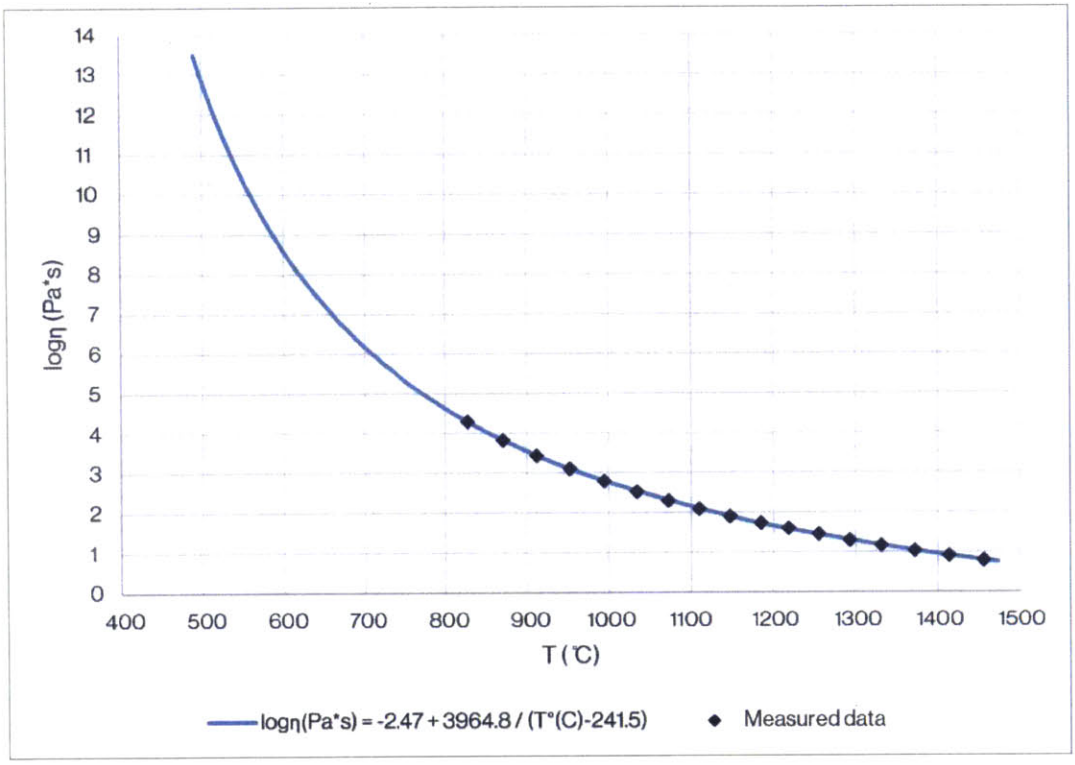

Figure 25. Experimental viscosity data and resulting VTF equation (Source: Corning Inc.)

3.2.2. PROCESS CHARACTERIZATION

3.2.2.1. TEMPERATURE DISTRIBUTION

Based on glass viscosity data, the operating temperature was set at approximately 1000°C, corresponding to the glass working point ($\eta \sim 10^3$ Pa·s). The nozzle temperature was set at T = 1010°C to account for the heat loss in the tip exposed to the annealing kiln environment. The crucible temperature was set at T = 1040°C to overcome the heat loss due to frequent refilling. The annealing chamber was set at T = 480°C, slightly below the glass annealing temperature (~515°C); since the glass heat radiation contributed to increase the environment temperature.

The temperature distribution in the system was simulated using Solidworks® Flow Simulation Computational Fluid Dynamics (CFD) software. Glass and refractories thermal properties were set as standard float soda-lime glass and 96% alumina respectively. Results are shown in (Figure 26A).

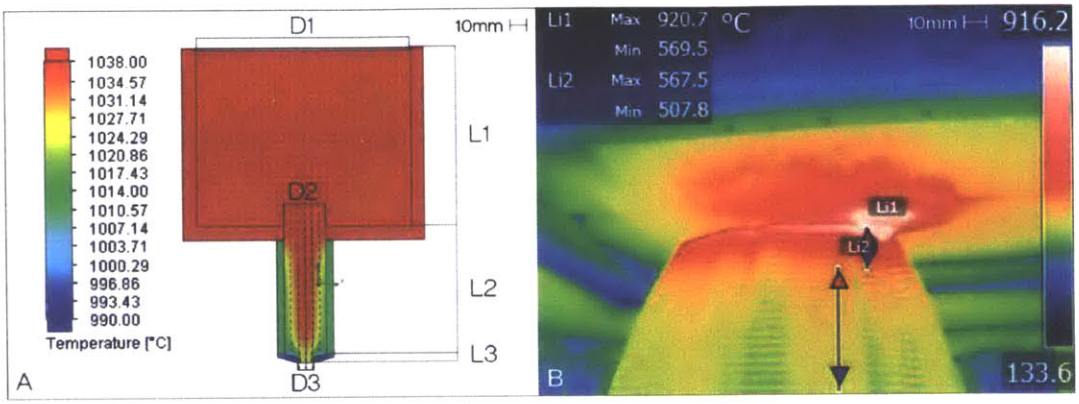

Figure 26. Temperature distribution as observed in the printing platform: (A) Solidworks® simulation of the crucible and nozzle assembly (with diameters and lengths of different sections highlighted) and (B) thermal image of an object being printed (Image credit: Forrest Whitcher)

Based on the CFD model, the temperature of the nozzle's outer face was expected to drop down to an average 980°C; the glass average temperature at the nozzle exit was 990°C.

Infrared images (Figure 26B) were acquired from the heated chamber window during a printing process using a FLIR T335 equipped with a T197000 high temperature option and were analyzed using FLIR Tools software (FLIR® Systems, Inc., Cambridge, MA, USA). At the nozzle exit, glass temperature was observed to be 920°C, in agreement with the simulations. Temperature decreased drastically as new layers were deposited, creating a temperature gradient of ~350°C between the most recent five layers. This led to a viscosity increase of five orders of magnitude. This rapid increase in viscosity was crucial to the stability of the object during printing.

Note that the object always remained in the 500-570°C temperature range, which corresponds to the annealing temperature of the glass in use; therefore, no cracks were formed during printing.

3.2.2.2. PHYSICS OF GLASS FLOW

Figure 27: Molten glass flowing through the heated nozzle (Image credit: Steven Keating)

The precise speed at which glass flowed through the nozzle (Figure 27) was an important determining factor for feed rate calibration helping to avoid undesired accumulation or lack of material on the printed object.

Glass flow through the nozzle can be modeled as laminar flow of a viscous fluid through a tube[21]. Whether a fluid under certain conditions will flow in a turbulent or laminar motion is a function of its density ϱ [kg/m3] and dynamic viscosity η [Pa·s] combined with its mean velocity v [m/s] and the channel diameter d [m]; Reynolds number Re is a dimensionless parameter which combines these factors and is used to help predict similar flow patterns in different fluid flow situations. Flow is assumed laminar if its Re falls below a threshold value of 204022.

In this case:

$$Re = \frac{\rho * v * d}{\eta} \sim 2.1 * 10^{-4} \quad (2)$$

The assumption of laminar flow was therefore largely justified; moreover, Re << 1 also indicates that viscous forces were predominant over inertial ones (Stokes flow)21.

The flow resistance of a tube is defined from the following relationship:

$$Q = \frac{\Delta P}{R} \quad (3)$$

where Q [m3/s] is the volume flowrate through the tube, ΔP [Pa] is the pressure drop at the top of the nozzle and R [Pa/(m3/s)] is the resistance to flow.

ΔP is given by the glass weight; for a cylindrical crucible:

$$\Delta P = \rho g \Delta h \quad (4)$$

Q can also be expressed by:

$$Q = A\frac{v_m}{2} = \frac{\pi r^4}{8\eta L}\Delta P \quad (5)$$

where A [m2] is the nozzle opening surface area, vm [m/s] is maximum flow velocity (at the center of the tube) and is two times the effective velocity, L [m] is the nozzle length and r [m] is its radius. The equation is known as the Hagen-Poiseuille law21.

R can therefore be calculated from:

$$R = \frac{8}{\pi}\eta\frac{L}{r^4} \quad (6)$$

There are two factors that determine the resistance to flow within the nozzle: geometry (primarily the nozzle's radius) and glass viscosity.

3.2.2.3. FLOW ESTIMATION

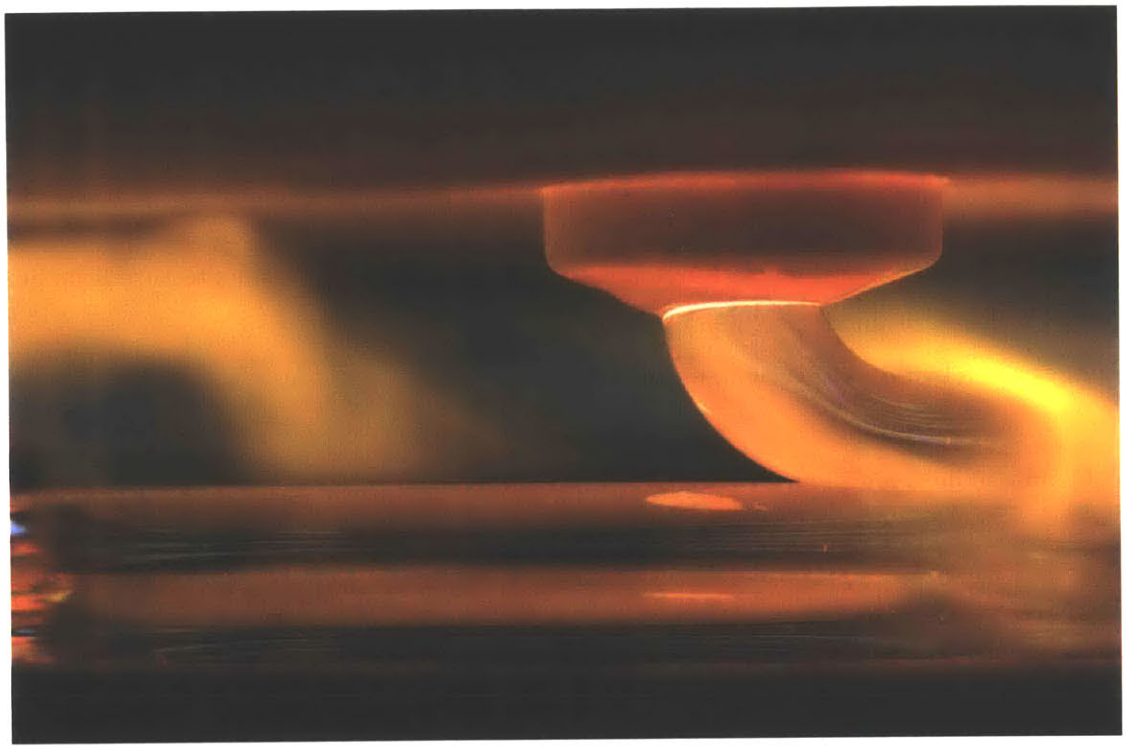

Figure 28: Molten glass exiting out of the nozzle at T ~990°C (Image credit: Steven Keating)

Based on previous equations, glass volumetric flow was estimated for typical processing parameters. Glass temperature at the nozzle exit (Figure 28) was considered to be T ~990°C, corresponding to a dynamic viscosity η ~640 Pa·s.

The pressure drop was a function of the molten glass level inside the crucible, since the process was gravity driven. The crucible-nozzle assembly is outlined in (Figure 17A). Designed lengths and diameters of crucible (1) and nozzle segments (2 & 3), along with correspondent flow resistances, are summarized in (Table 4).

Table 3. Flow resistance in the crucible and nozzle assembly.

	L (mm)	D (mm)	R [Pa/(m³/s)]	R [%]
1	100	120	$8.23 \cdot 10^5$	0.1%
2	73.5	23.5	$4.11 \cdot 10^8$	44.5%
3	3	10	$5.12 \cdot 10^8$	55.4%
Total	176.5	-	$9.24 \cdot 10^8$	-

Based on the knowledge that the final smallest diameter drives the overall flow resistance, the length of the final segment was minimized. (Table 4) shows that more than 50% of the flow resistance (R) was given by the final segment of the assembly.

For this calculation, it was assumed that at the start of a new print job the crucible was filled up to a height of L' = 80mm, resulting in a pressure drop of $\Delta P \sim 3.6$ kPa. Volume flow rate at the nozzle exit was therefore $Q = 460\, mm^3/s$ with a consequent linear flow rate of $\bar{v} \sim$ 5.7 mm/s.

As the glass level in the crucible decreased, Q and $\bar{v}$ decreased linearly; consistency during printing was achieved by frequent refilling of the crucible. The extended nozzle enabled direct deposition of material referenced from the machines Z-height, rather than previous layer height, thus any variation in flow rate would affect the wall width rather than the path height.

We estimated the flow rates instead of simulating because modelling the system working regime is an incredibly difficult task. First, it involves setting up a robust CFD and thermodynamic engines for the simulation environment. Second, glass is challenging to model due to the inherent material properties (it transitions from a liquid to solid-like state through the process) and would require a viscofluid simulation. During the printing process, the glass passes through three heated environments and is altered by each. As the molten glass passes through the nozzle orifice it is exposed to a ~500 °C temperature drop. This change of temperature increases the viscosity allowing the glass filament to maintain its shape. Radiant and convection heat accumulates in the lower print chamber and around the printed object. Additionally, heat is transferred through conduction of the previous print layer. This heat build-up causes the print layers to slightly reduce their height in the Z axis. This would need to be accounted for in order to create an accurate model. Furthermore, it is difficult to get accurate temperature viscosity curves (the key data for establishing a model) for any glass composition, and we unfortunately did not receive ours till the end of the first phase of the project.

3.3. FABRICATION OF 3D PRINTED GLASS PARTS

3.3.1. METHOD

Two methods for filling the Crucible Kiln were employed. In the first method, glass nuggets were heated in the crucible to 1165°C over 4 hours; glass was then fined for 2 hours to eliminate bubbles. During this phase, the nozzle was kept at a lower temperature (T~800°C) to prevent

glass flow. In the second method, molten glass was collected from a furnace and added directly to the crucible.

After fining, the crucible and nozzle temperatures were set to 1040°C and 1010°C respectively. The Print Annealer was also set to 480°C. Glass flow typically initiated spontaneously due to gravity; however, flow could be terminated at the end of each print by cooling the nozzle tip with compressed air and reinitiated at the beginning of the following print by heating the nozzle tip with a propane torch.

Once the printing process was complete, the crucible and nozzle were drained by increasing their temperature up to 1165°C. The Print Annealer then executed the annealing cycle as summarized in (Table 5).

Table 4. Annealing cycle.

Cooling rate (°C/h)	T (°C)	Dwell time (h)
-	480	1
25	400	-
50	150	-
50	80	-
120	20	-

For increased part production other annealing kilns were used; objects were removed through the front door and placed in an external annealing kiln kept at 480°C until the end of the multiple printing session. They were then annealed following the same cycle.

Most objects were post-processed in order to be properly displayed: sharp edges where the print was terminated were ground and bottoms were polished to eliminate the roughness caused by the contact with the build platform during printing.

3.3.2. PARAMETERS CALIBRATION AND DESIGN SPACE

"Brick says: I like an arch."
-Louis Kahn

The printing process was tailored according to the temperature and resultant viscosity and flow rate. Two different sets of parameters were used:

- Tnozzle = 1010°C, layer height = 4.5mm, feed rate = 4.5mm/s
- Tnozzle = 1010°C, layer height = 4.5mm, feed rate = 6.1mm/s

The first set of parameters was associated with a feed rate that was 20% slower than the estimated flow rate. This resulted in layers with a much larger width compared to the nozzle diameter; the average layer width of the printed parts was w1 = 19.5 ± 3.5 mm. A top view of a printed object is shown in (Figure 29A). [Note: direct measurement of layer width was challenging; therefore, width was calculated based on the object's mass, layer height, feed rate and printing time].

Printing with this large layer width required a considerable amount of glass and therefore limited the design space. The second set of parameters was calibrated to achieve a smaller width, similar to the nozzle's orifice.

Different feed rates were tested in the range 5.8 – 6.3mm/s, while keeping the other parameters constant, an optimum feed rate = 6.1mm/s (~7% higher than the flow rate) was determined. Driving the extruder at a slightly greater rate than the natural flow helped achieve a more homogeneous filament, since the pulling prevented the buildup of any excess glass at the nozzle. In order to achieve effective adhesion of the first printed layer to the building platform, its feed rate was slowed down by 25%, eliminating the pulling force and giving the glass time to settle on the build platform. The second set of parameters resulted in an average width of t2 = 9.5 ± 0.5mm, roughly half of what was produced with the first set. This approach enabled the production of larger and taller objects with the same amount of glass; the pressure head variation was more gradual and easier to control by frequent refilling. (Figure 29B) shows a top view of an object printed with the new set of parameters; (Figure 29A) and (Figure 29B) highlight the difference between layer widths.

Improved control achieved with the new set of parameters allowed for the exploration of various other possible designs. In the optimal printing conditions (clean nozzle, proper set of parameters) parts with draft angles up to 40° and turning radii down to 14mm were printed.

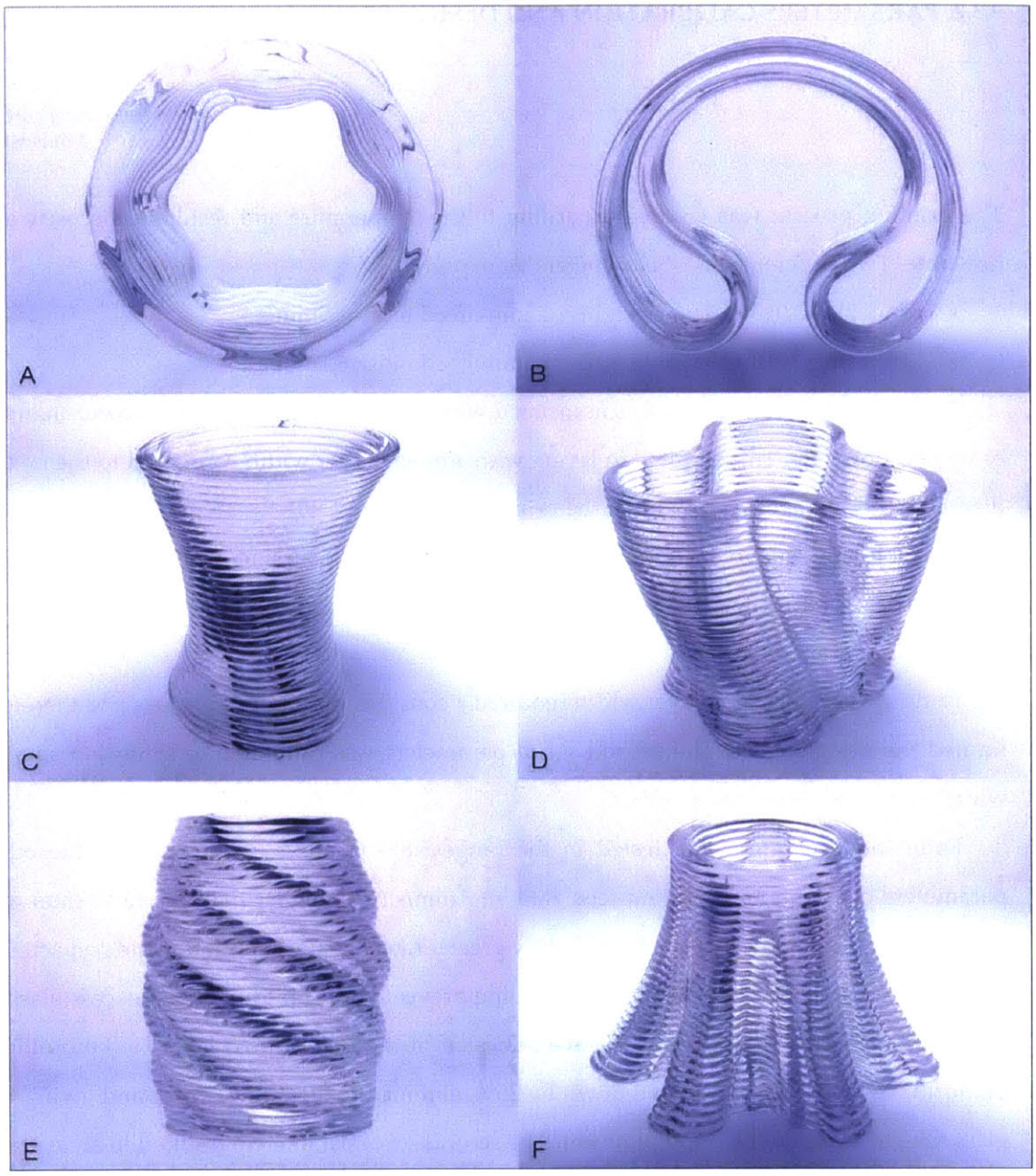

Figure 29. Objects printed using the platform. (A) Parameters set (PS) 1, layer width; (B-F) PS 2, exploration of design space: (B) large radii, no drafting, focus on layer width; (C) smaller radii, higher drafting; (D) same as (C) but with changes in concavity/convexity in plane; (E) changes in concavity/convexity out of plane; (F) smallest radii and highest draft angles (Image credits: Chikara Inamura)

Table 5. Printed objects parameters and features.

	A	B	C	D	E	F
Nozzle T (°C)	1010	1010	1010	1010	1010	1010
Feed rate (mm/s)	4.5	5.8	6.1	6.1	6.1	6.3
Printing time (min)	22	39	34	39	37	44
Layer height (mm)	4.5	4.5	4.5	4.5	4.5	4.5
Layer width (mm)	23.4	9.7	9.4	12.8	9.3	8.9
Min. radius (mm)	16	30	22	28	21	8
Max. draft angle (°)	20	0	28	29	28	32

The exploratory designs shown in (Figure 29B-F) (characteristics listed in (Table 6)) represent increasing levels of complexity and focus on different design objectives. The object in (Figure 29B), for example, was not challenging in terms of minimum radius or draft angle, but investigated the possibility to fabricate thin channels and cavities by decreasing the distance between walls. (Figure 29C) shows a more complex object, with a minimum radius of 22mm and a draft angle of 28°, which was successfully produced.

Working in a safe design space did not always produce defect-free objects. Radii and draft angles were not the only constraints that affected the quality of the print. Object in (Figure 29D) had a minimum radius of 28mm and a draft angle of 29°; nevertheless, defects were observed in its bottom layers. It was determined that changes of convexity within the same layer often resulted in deviation from the CAD shape. This effect was caused by accumulation of glass on the nozzle tip and out of line pull force caused by surface tension between the glass on the nozzle face and the just deposited glass.

This phenomenon could be avoided by creating geometries where the change in convexity occurs not within a single layer but instead over the height of the part: a successful example is shown in (Figure 29E) in comparison to that of (Figure 29D).

The last object (Figure 29F) was the most ambitious, printed with a minimum radius smaller than the nozzle diameter and abrupt changes in curvature. Deviations from the designed path followed a regular and repeatable pattern in the symmetric branches of the part.

3.3.3. FALLING FLUID DEPOSITION

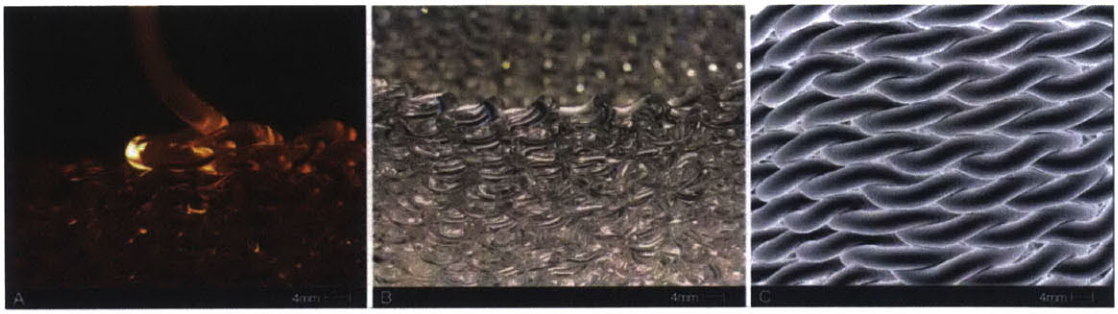

Figure 30. Falling Fluid Deposition: (A) deposition process (Image credit: Steven Keating), (B) detail of the printed object and (C) detail of the microCT scan (Image credit: James C. Weaver)

Molten glass deposition from an offset may form a plethora of patterns when the relative speed of nozzle and substrate is lower than the impinging speed of the falling glass; those patterns include meanders, W patterns, alternating loops and translated coiling. This phenomenon is of particular interest given the opportunity to fabricate multiscale objects where the features generated by coiling are at a much smaller scale than the motion of the printer. Viscous threading has been the subject of several studies involving a fluid falling on a moving belt and is often referred to as the "Fluid Mechanical Sewing Machine"[23–25]. Brun, P.-T. et al.[26] recently developed a model to rationalize the rich variety of periodic patterns generated in terms of two parameters: the dimensionless height of fall H and the dimensionless velocity or travel speed V, which take into account the balance between gravitational stretching and viscous dissipation. For a thread, in this case glass, of kinematic viscosity ν [m2/s] falling from a nozzle of dimensional height H· onto a belt horizontally moving at speed V·, it is:

$$H = H^* \left(\frac{g}{\nu^2}\right)^{1/3} \tag{7}$$

$$V = \frac{V^*}{(\nu g)^{1/3}} \tag{8}$$

Based on this behavior, a cylinder with the following set of parameters was printed:

Tnozzle = 1070°C, layer height = 4.5mm, feed rate V· = 6.1mm/s, offset height H· = 100mm, H = 1.02 and V = 0.003.

This resulted in the formation of a translated coiling pattern that followed the circular path to form a complex cylinder. Details of the deposition process and of the object can be seen in (Figure 30A-B).

The object was imaged by means of micro Computer Tomography (microCT) with an XRA-002 X-Tek MicroCT (Xtek Inc., Cincinnati, OH, USA) system in order to better visualize the generated patterns. The 3D reconstructions were performed using CT-Pro (Nikon Metrology Inc., Brighton, MI, USA); surface renderings were generated using VGStudio Max (Volume Graphics GmbH, Heidelberg, Germany).

From the 3D reconstruction shown in (Figure 30C), the generated loops seemed to be consistent in their radii and spacing.

3.3.4. COLORED GLASS PRINTING

Colored glass has been investigated since the very early stages of material exploration. One of the goals was to control the optical and aesthetic properties of the printed glass structures through the integration of color. Preliminary tests demonstrated the effective printing with multiple glass colors in the same object.

Two variations of glass frits were used: Reichenbach R-19 Gold Topaz, F0 frit size (less than 1mm), and R-11 Heliotrope in F2 size frit (2-4mm) (Farbglashütte Reichenbach GmbH, Reichenbach, DE).

The frits were added in sequence to the crucible, which was partially filled with molten glass. Due to the relatively low melting point and mass, the frits melted within minutes. (Figure 31) shows a detail of the resulting object. Both a sudden change and a graded conversion from one color to the other were possible within the same printed object. The printing process was not noticeably affected by addition of the colored frits.

Figure 31. Detail of a colored printed object; both a sudden change in color (top ring) and a graded conversion (bottom) are visible (Image credits: Chikara Inamura)

3.4. CHARACTERIZATION OF 3D PRINTED GLASS PARTS

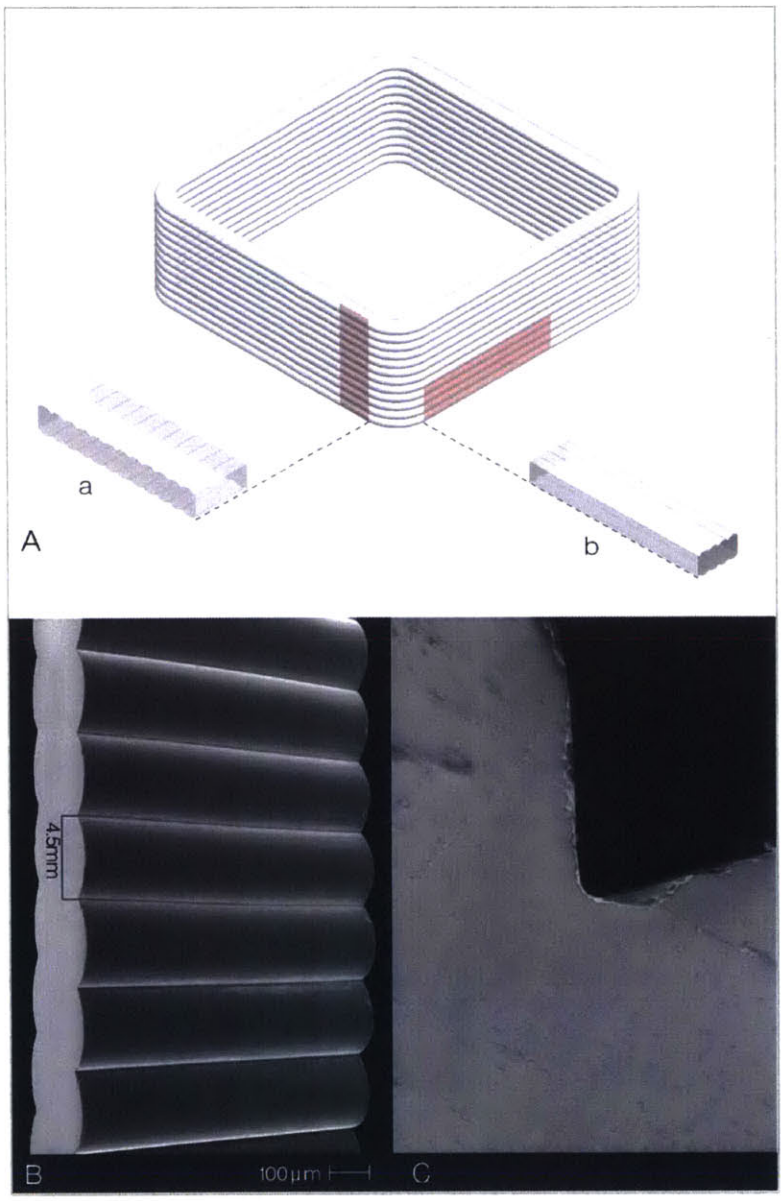

Figure 32. Characterization of the printed parts. (A) Samples production from a printed prism; (B) SEM image of type a sample; (C) SEM image of the interface between two layers on a type a sample (Image credit: James C. Weaver)

Rectangular prisms were 3D printed and then cut down with a diamond saw to provide samples for optical and mechanical characterization. The cut surfaces were diamond ground and polished with cerium oxide.

A number of rectangular prisms were printed at room temperature (T0) and then annealed; others were printed into the Print Annealer (Ta).

Samples were cut in different orientations: some of the bars (a in Figure 32A) were cut with the longer axis along Z-direction and others (b) with the longer axis along the X (or Y) direction. The samples height corresponded to the layer width. A representation of the samples and their specifications are shown in (Figure 32A) and Table 7, respectively.

Table 6. Samples specifications.

	a.T_0	b.T_0	a.T_a	b.T_a
T (°C)	25		482	
layer height (mm)	5.5		4.5	
width (mm)	10.8 ± 0.8		9.8 ± 1.0	
length (mm)	56.1 ± 1.8	78.0 ± 1.2	56.1 ± 1.8	78.0 ± 1.2
base (mm)	17.7 ± 0.6	18.4 ± 0.4	17.7 ± 0.6	18.4 ± 0.4

3.4.1. SCANNING ELECTRON MICROSCOPY (SEM)

Samples were sputter-coated with gold and imaged with a Tescan Vega SEM (Tescan Orsay Holding, a.s., Brno-Kohoutovice, Czech Republic) and a FESEM Zeiss Ultra 55 (Carl Zeiss, Inc., Thornwood, NY, USA). Images of an a.Ta sample are shown in (Figure 32B-C).

The images demonstrate that the object's section was highly homogeneous with strong adhesion between the layers. (Figure 32C) shows an enlargement of the contact surface between two layers, with a smooth, blunt interface where no sign of the different layers was visible.

3.4.2. RESIDUAL STRESSES – POLARISCOPY

The samples were observed under a Model 243 6" Polariscope with Tint Plate (PTC® Instruments, Los Angeles, CA, USA) to determine residual stress patterns developed during glass cooling.

Polariscopy is a well-known technique in glass industry as it takes advantage of stress-induced birefringence in glass to detect the presence of residual stresses mainly due to cooling gradients[27,28]. As polarized light travels through glass, it undergoes a delay proportional to the amount of stress. Therefore, color fringes visible through the analyzer mimic the stress pattern. Color and line intensity are not absolute, but depend on the orientation of the sample and the

polarized filters. The results were obtained through qualitative reading of the color fringes with no quantitative evaluation of stress intensities.

Both samples printed at T0 and Ta showed negligible stress concentration along the layers, indicating that the annealing treatment was successful. Looking at the cross-sections, though, a difference between the two kinds of samples was detected. Printing at room temperature generated radial stresses within layers that had not been relieved by the subsequent annealing treatment. In the sample fabricated with the Print Annealer, on the other hand, such stresses were not present and the stress distribution was more homogeneous.

3.4.3. PRELIMINARY MECHANICAL TESTING

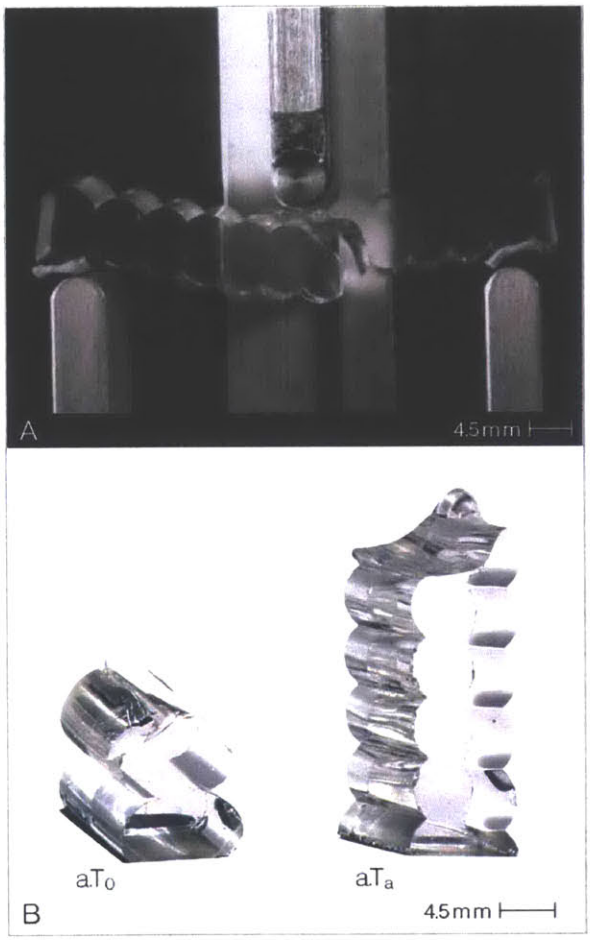

Figure 33: (A) 3 points bending test on a a.T_a sample (Image credit: Kyle Hounsell); (B) samples a.T_0 (left) and a.T_a (right) after fracture.

Residual stress patterns suggested that samples printed into the heated chamber possessed better mechanical properties compared to the ones printed at room temperature. The flexural behavior of the glass bars was investigated using an Instron 8841 and an Instron 5500R (Illinois Tool Works Inc., Glenview, IL, USA) equipped with a 3 points bending fixture. Tests were performed at a cross-head speed of 0.05 to 0.12mm/min. A compliant layer (Scotch® Permanent Outdoor Mounting Tape, 3M, Saint Paul, MN, USA) was used between the bottom fixtures and the sample surfaces in some orientations. Results are reported descriptively due to the limited number of samples examined.

(Figure 33A) shows a sample loaded along the layers; this is usually the most critical loading configuration for a 3D printed object, because delamination can occur due to a poor adhesion between layers[29–31]. The tests conducted on a.T0 samples seemed to validate this hypothesis: the fracture occurred at the interface between two layers ((Figure 33B), left) and the samples possessed a flexural strength σf which was only one fifth of the one of the annealed samples a.Ta. This was most likely due to lower bonding strength caused by the large temperature difference between the deposited glass and the previous layer and to the presence of residual stresses between layers, as highlighted in Residual Stresses - Polariscopy. The absence of high residual stresses in a.Ta samples resulted in fracture lines that propagated through a whole glass layer without following a precise trajectory ((Figure 33B), right), a further indication that no significant residual stresses were present in the sample.

Additionally, in the annealed samples flexural strength measured in the a and b type orientations differed by approximately 40%. This level of anisotropy is in line with what has been observed in plastic printed parts in other studies[32].

3.4.4. OPTICAL PROPERTIES

One of the main goals of this work was to combine additive manufacturing processes with the production of glass components possessing desirable optical properties.

Morphological and mechanical characterizations determined an overall high degree of homogeneity and good adhesion between layers, enabling light transmission with very little distortion. The 70mm tall cylinder shown in (Figure 34A) was polished with cerium oxide in both top and bottom layers; a high degree of transparency could be observed.

If layer surface texture was retained, it enabled light refraction and scattering as well as the production of highly complex caustic patterns. Images shown in (Figure 34B) were obtained by lighting the objects along their central axis using a LED. The optical properties are shown form a selection of objects in (Figure 35 - Figure 40).

The observed behavior offered new perspectives on light control and additional optical properties for the printed objects. Work by Kiser et al. has shown that precomputed shapes can be generated with caustics by modeling light transmission to control the patterns and form desired shapes providing future directions for this work to explore[33].

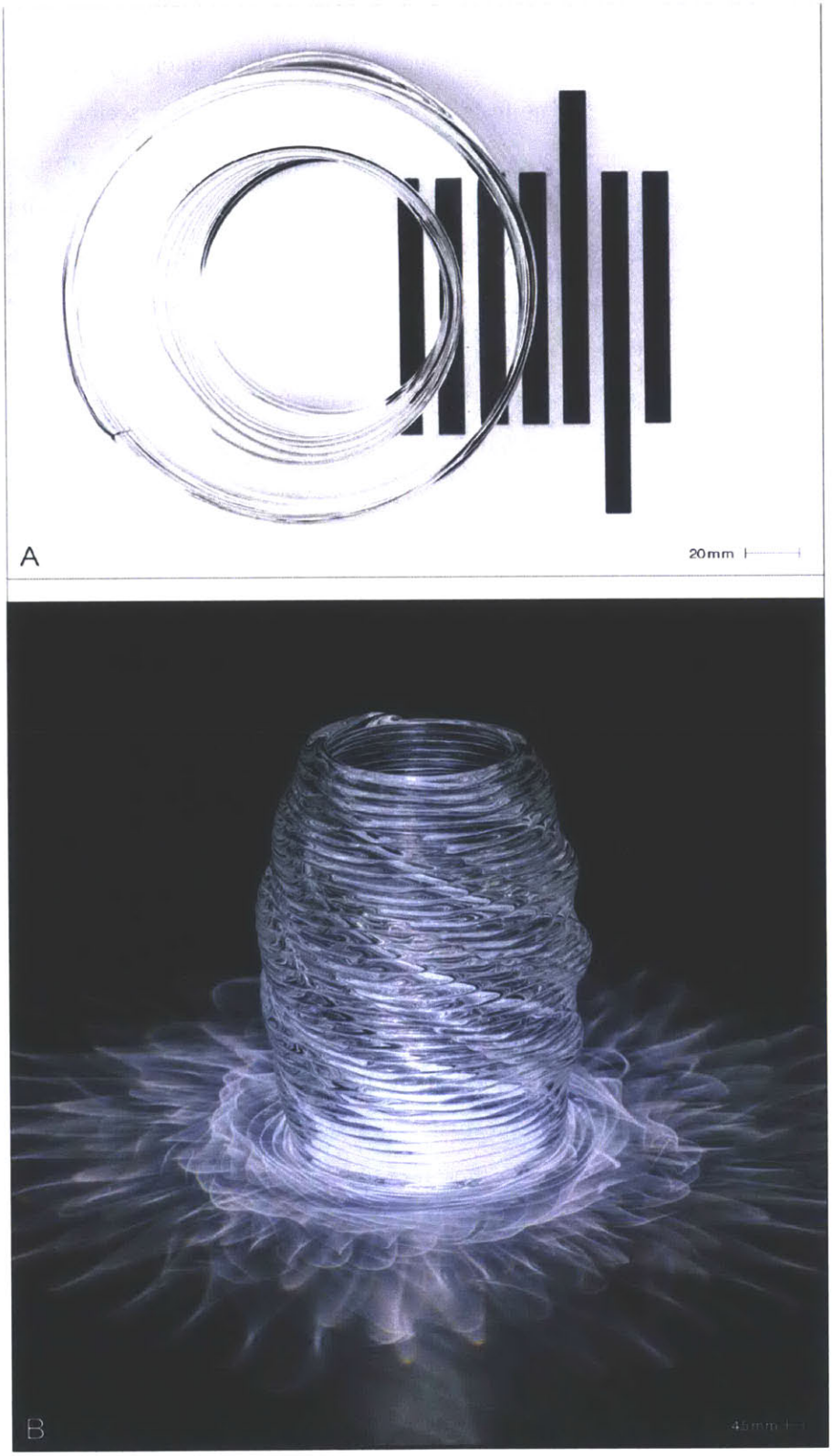

Figure 34. Optical properties and caustic patterns of printed parts. (A) Top view of a 70mm tall cylinder showing a high level of transparency; (B) caustic patterns created by illumination from a suspended overhead LED (Image credit: Andy Ryan)

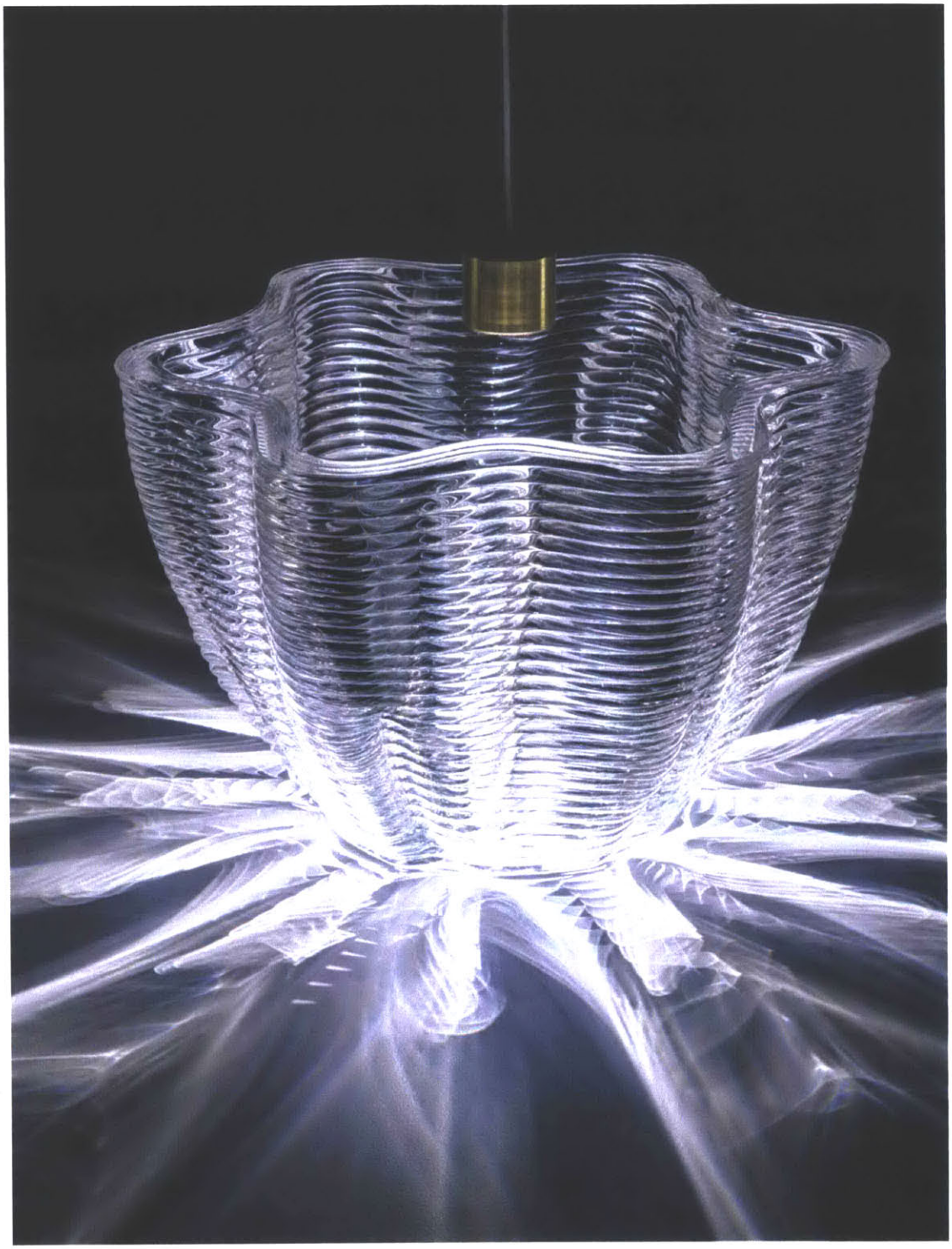

Figure 35: Caustic patterns created by illumination from a suspended overhead LED (Image credit: Andy Ryan)

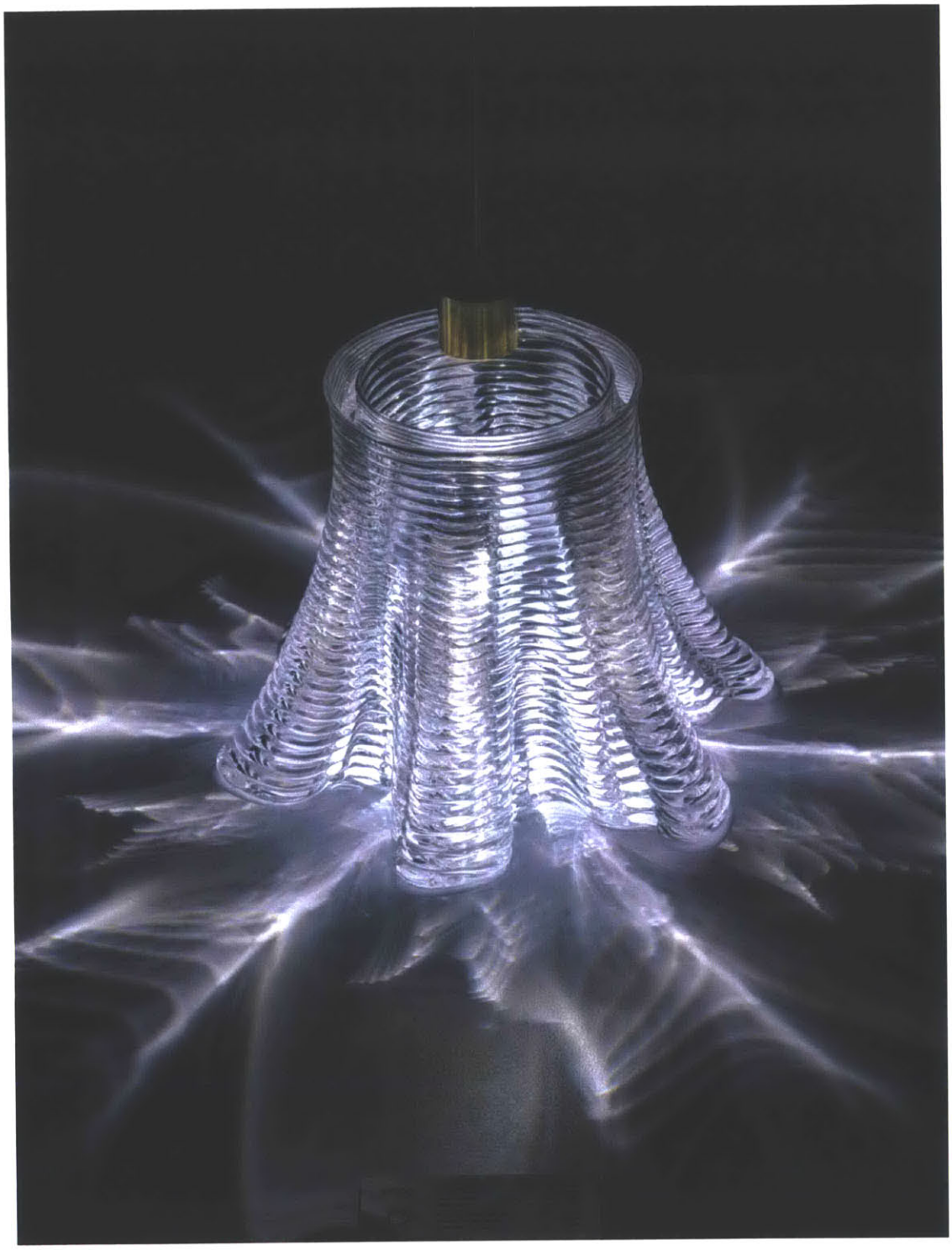

Figure 36: Caustic patterns created by illumination from a suspended overhead LED (Image credit: Andy Ryan)

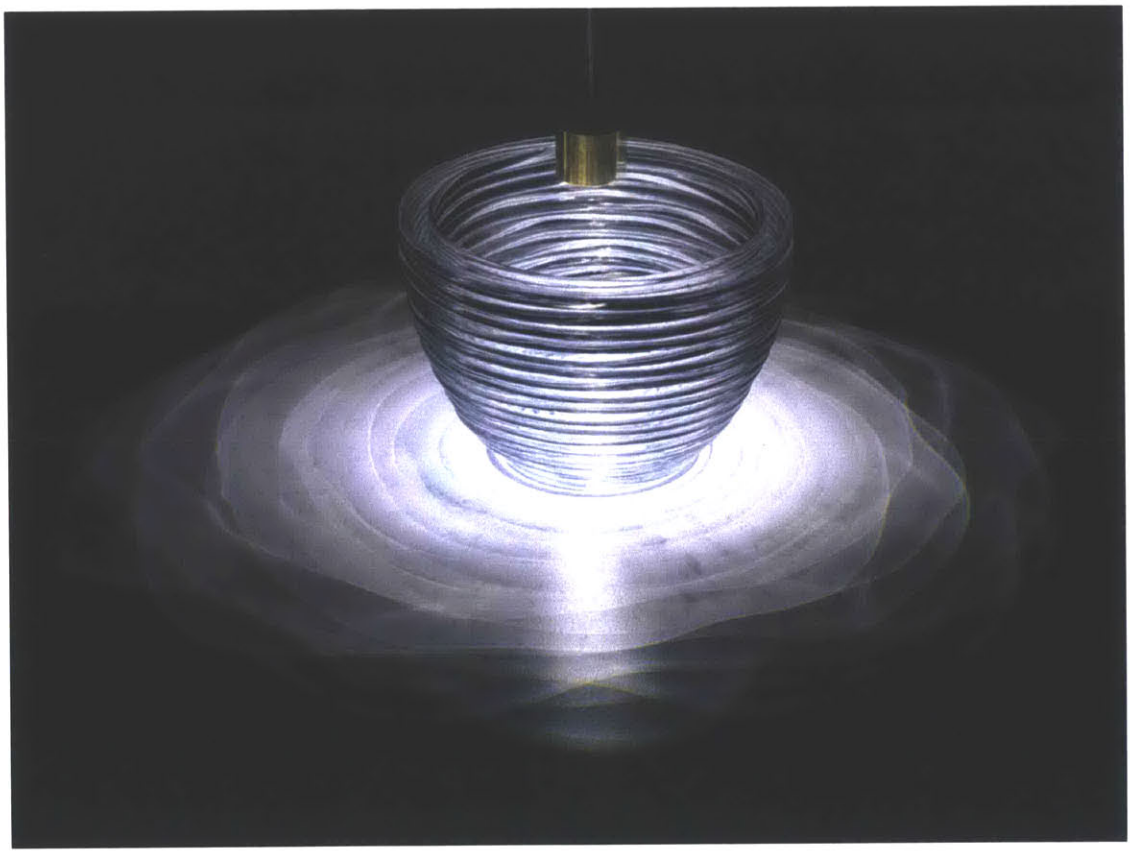

Figure 37: Caustic patterns created by illumination from a suspended overhead LED (Image credit: Andy Ryan)

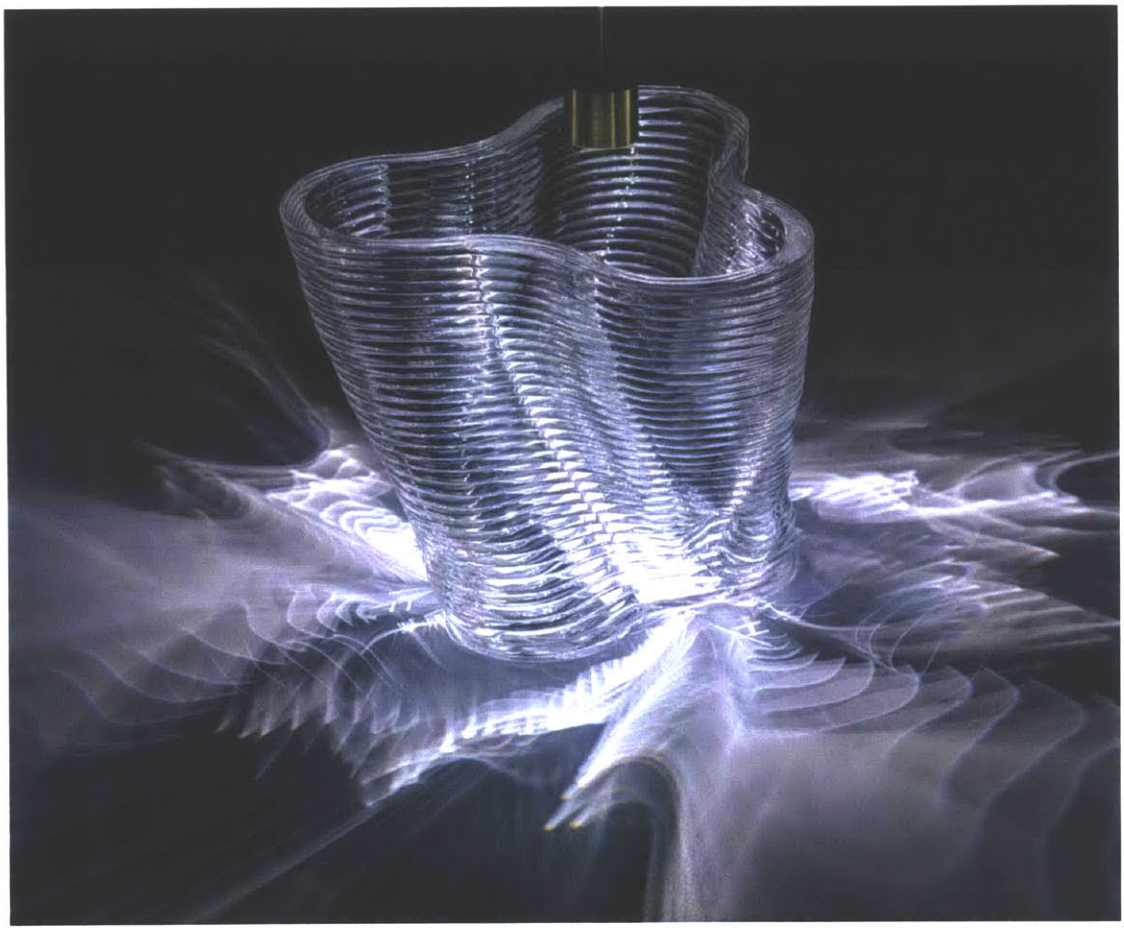

Figure 38: Caustic patterns created by illumination from a suspended overhead LED (Image credit: Andy Ryan)

Figure 39: Caustic patterns created by illumination from a suspended overhead LED (Image credit: Andy Ryan)

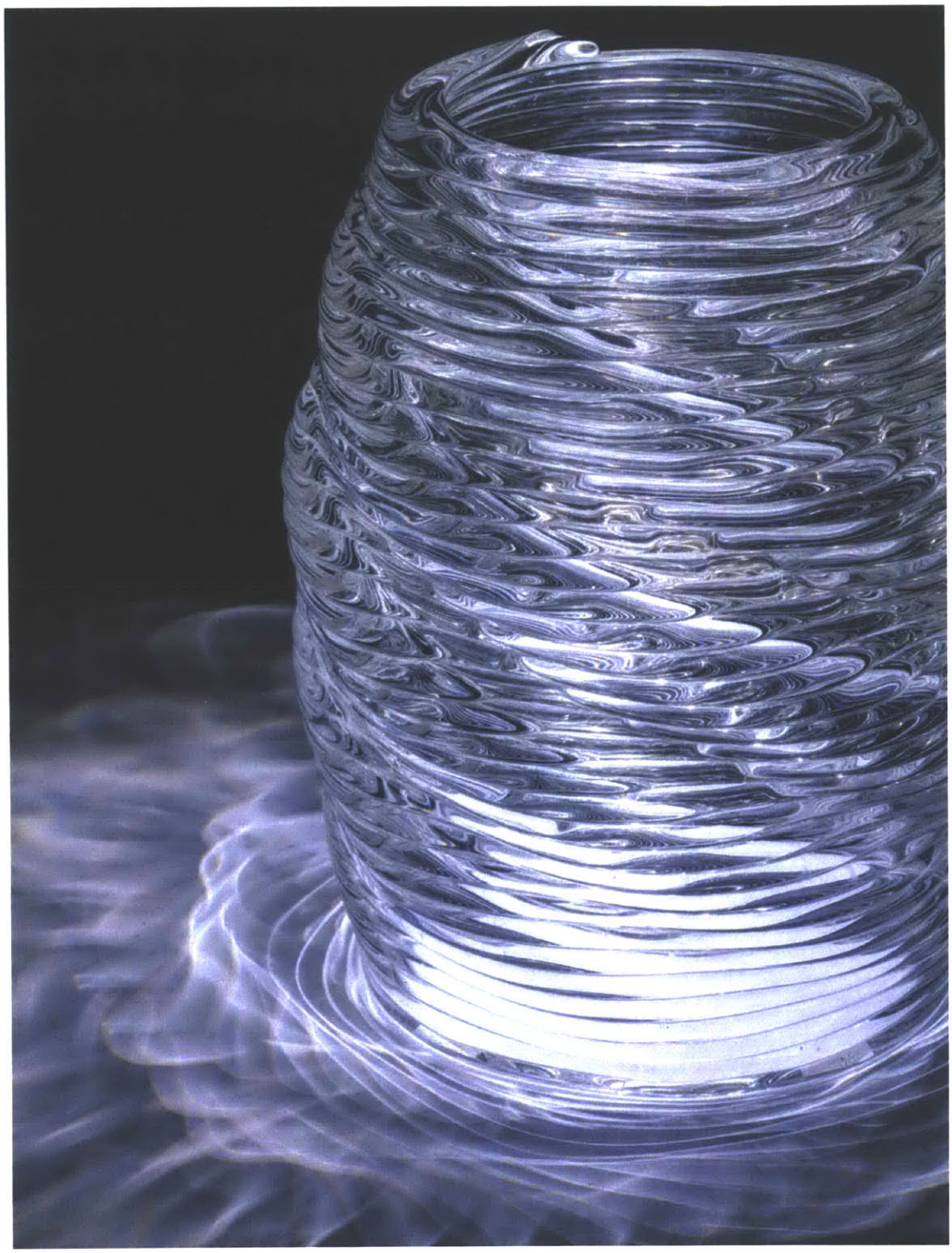

Figure 40: Caustic patterns created by illumination from a suspended overhead LED (Image credit: Andy Ryan)

3.5. LIMITATIONS AND FUTURE WORK

The focus of the present work was to demonstrate the functionality of a molten glass material extrusion system; initial work focused primarily on the printer construction and process calibration to this end. There are many different directions for future work that arise based on this first glass 3D printer.

Only preliminary testing was conducted on the printed glass objects. More comprehensive morphological, mechanical and optical characterizations of printed components are underway and future work will validate the qualitative observations through more accurate and extensive testing.

The printer here presented is still in development and there are a number of improvements that are currently being carried out. For instance, extruded glass stuck preferentially on glass covering the nozzle tip instead of on the colder previous layer; such phenomenon was responsible for the deviation from desired shapes and uneven glass distribution. Future work on the printer will focus on solving this issue. Numerous potential solutions will be tested by creating new nozzle geometry, material, coating, face cooling or the addition of sacrificial foil. Software environment improvements will be explored to merge the large number of separate pieces of software needed to run the system. This will enable the operator to have full control of printing process in real time, including direct control over the kilns' temperatures and path modification and travel speed, from the same interface.

Gravity as a feed mechanism required frequent refilling of the crucible, needed to keep the glass level almost constant. This procedure affected the quality of the print - from nearly imperceptible to those observable with the naked eye. Having a continuous flow of material in the feeding chamber would allow the realization of more homogeneous parts.

The relatively small pressure drop generated by the gravity fed system was also a limiting factor in terms of printing speed and resolution, and also prevented scaling down the nozzle diameter. Future development will therefore involve the addition of an active material feed system (in the form of a plunger or of compressed air) in order to increase control and enable a more diverse set of parts to be fabricated at a faster rate and with finer resolution.

The printer development was carried out using soda lime glass, chosen because of its relatively low working temperature and wide working range. Our method could be applied to a diverse range of materials, including other silicate, borate and phosphate glasses as well as

glass-ceramic systems and potentially Lunar and Martian soil. In order to process these materials, a future version of the printer would thus be able to heat glass to higher temperatures.

To fully achieve the level of complexity of AM processes this system requires the ability to automatically start, stop and cut the glass filament. In the current setup, these tasks are manually activated by the operator. Multiple different mechanisms to achieve this level of control are being explored from automating the compressed air and torching that currently performed manually to adding shears or a high temperature valve. The addition of these features would expand the design space enabling the creation of designs with intricate cross-sections and internal structures.

Initial efforts are being conducted to see how and why the technology could be utilized to manufacture an architectural system from printed glass components. As a starting point, we are beginning to compare the 3D printing approach to conventional glass pressing methods, which are used to manufacture glass building components. This is a very complex exercise to undertake, given that we have only built one prototype of the 3D printing system, and press manufacturing has evolved throughout the 20th century into a well-established industrial process. The first step requires a framing of the problem, and in our case, we made three assumptions:

1) We assume that both processes require the same cost and energy to prepare the molten glass for forming. This includes furnace and glass feeding setup, raw material extraction and processing, batch transportation and delivery, a batch feeding mechanism, and a glass fining period.
2) We assume that a simplified press manufacturing platform could be built at the same machine scale and costs as our 3D printing platform
3) We assume that both processes require the same cost and energy to anneal the produced components.

The three assumptions enable us to now to isolate the process from the entire life cycle of production. The preliminary study proceeds to compare the fabrication of a 2.26 kg glass component through our 3D printing process and a conventional glass pressing method.

Glass blocks made by a press manufacturing approach have advantages in terms of the amount of time it takes to make a component (~1 minute), which results in high-throughput production. This approach, however, is limited in its ability to produce complex components

with internal features, and has a highly constrained design space. Press manufacturing results in the mass production of a single design due to the dependency on a mold, and often builds bulkier objects.

The biggest disadvantage to 3D printing a glass component is that it is ~30x slower than press manufacturing. The advantages with 3D printing are in the expanded design space, the ability to achieve mass-customization, and the fact that design complexity can be achieved. Glass can be distributed in a more sophisticated way throughout the cross section of each component, and intricate inner features are feasible. 3D Printing enables you to customize on the fly, eliminate the need for tooling and industrial scale molds.

Each approach has its own constraints, and choosing one over the other is a matter of trade-offs. Figure 41A compares the fabrication energy, time and energy cost per component between the two processes. Two graphs in Figure 41B compare the data and preliminary analysis in an Energy vs Time and Customization vs Complexity graph.

This argument reveals that the invested energy in printing is lower, despite the slower speed, and that the ability to create custom complex objects is much higher. As there is numerous variables that could influence this result, it demonstrates that there is not an order of magnitude difference in energy consumption of the two processes.

Evaluating the scope between the two processes is a rather difficult task, and these preliminary results are one of many approaches. Much more work needs to be conducted to provide concrete analysis.

Energy Quantification	
Glass Properties	**Value**
Price	1.7 USD / kg
Density	2.52 g/cm³
Molding energy *(Source: Asbhy)*	9.20 MJ/kg
Machine Power	
Crucible Kiln	1800 W
Nozzle Kiln	300 W
Print Annealer	3000 W
Motors & Electronics	20 W
Total Watts	5120 W
Object 3D Print Time	1800 W
Total Machine Energy to Print	9.22 MJ
Energy Required for Heat Transfer to Soda-lime Glass	
Volume of the crucible:	1447.63 cm³
(m) Mass of material	2260.00 g
(c) Specific Heat of soda-lime glass	0.75 J / g°C
(Δt)Change in temperature 1040°C - 25°C	1015.00 °C
Q (energy required to transfer heat) = mcΔt	1.72 MJ
Total Energy to 3D Print 1 glass object	10.94 MJ
Total Energy to Mold 1 glass object	20.79 MJ

Comparison: Printed vs Pressed Glass Block		
Item to compare	**3D printed block**	**Pressed block**
Dimensions	Variable	19x19x8 cm
Weight	2.26 kg	2.26 kg
Fabrication Time	30 min	1 min
Cost of 2.2kg of glass	$3.84	$3.84
Energy	11.2 MJ	21 MJ
Energy conversion: MJ > kWh	3.113 kWh	5.776 kWh
Cost of energy per object *(US average 12cents per kWh)*	$0.37	$0.69

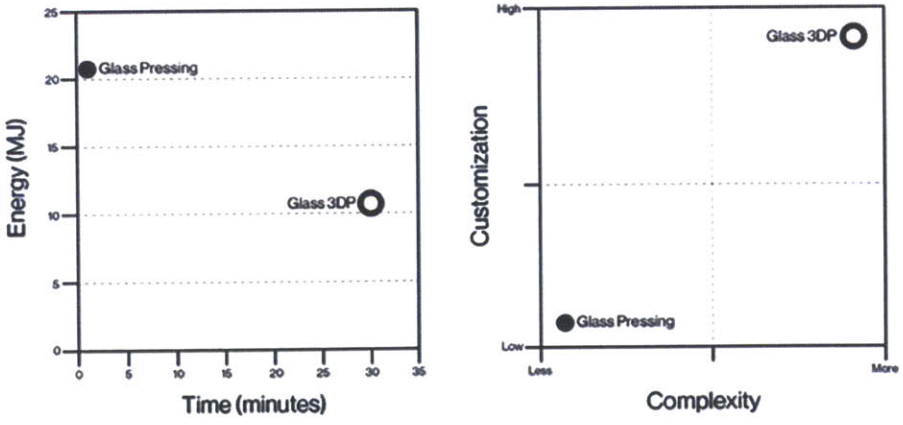

Figure 41: (A-Top) A chart outlining preliminary attempts at quantifying the energy required for the 3D printing and press fabrication approaches (B-Bottom) Energy vs Time graph and Customization vs Complexity graph between the two approaches

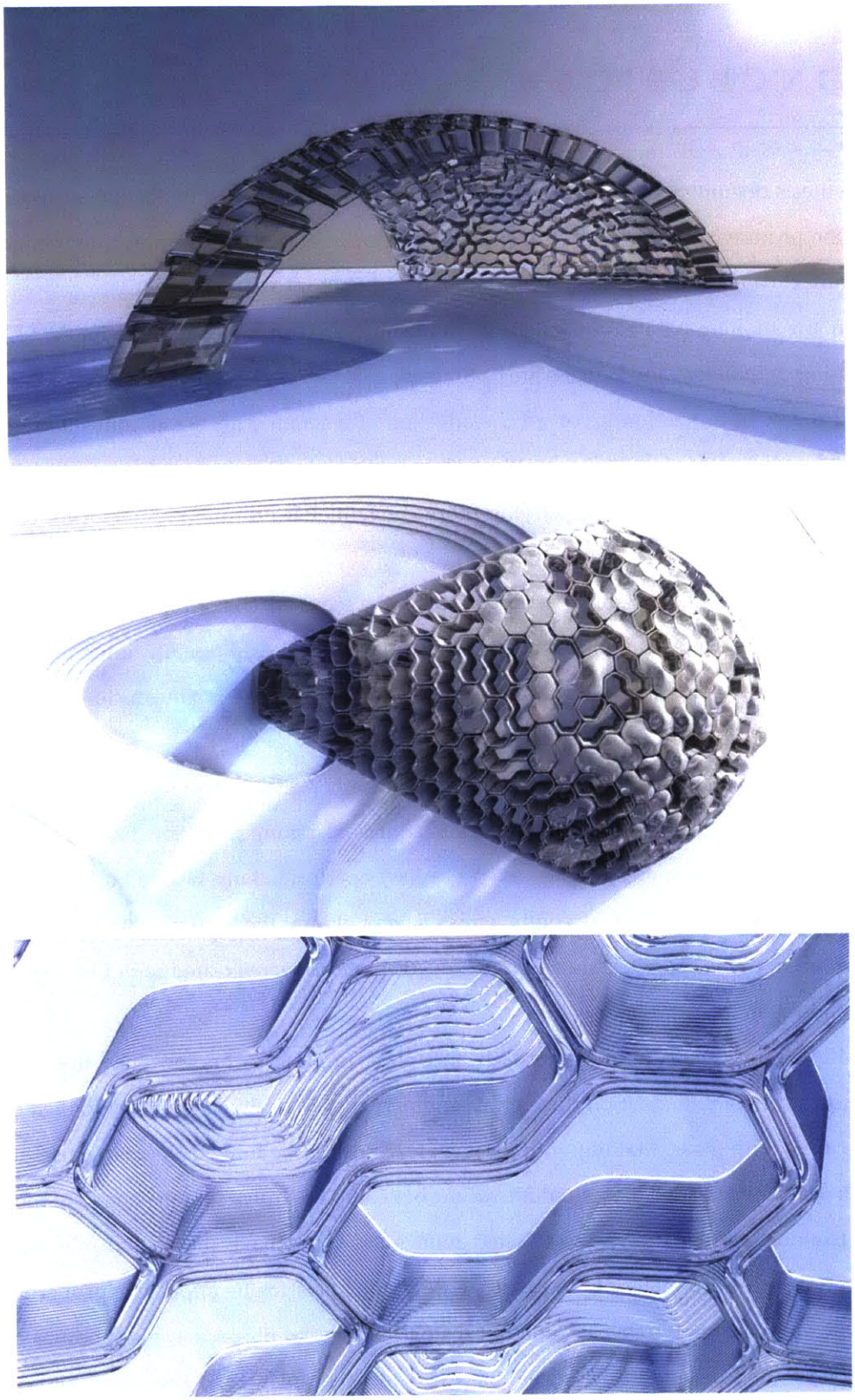

Figure 42: Conceptual design for a compressive shell structure with 500 3D printed custom glass components

CONCLUSIONS

The thesis documents the development of the first molten glass material 3D extrusion system for the production of optically transparent components, and builds upon 5,000 years of glass manufacturing traditions to offer a new fabrication approach. This system processes glass from the molten state to annealed components of complex digitally designed forms. The printing parameters and process are optimized, enabling high repeatability and control.

Process optimization involved the addition of a ceramic nozzle of controlled geometry, modeling the glass viscosity, controlling glass levels, adjusting the temperature distribution in the different kilns, as well as varying more conventional printing parameters such as layer height and feed rate.

The design space enabled by this system was mapped, including geometric constraints such as maximum overhang and minimum turning radius. Additionally, integration of colors was shown to be possible and the generation of coiling patterns as a means to produce objects of multiple different length scales was investigated.

Preliminary printed material characterization was performed in terms of morphological, mechanical and optical properties. Results indicated strong adhesion between layers and substantial strength increase when the process was performed in a heated build chamber with roughly 60% of material strength across layers. From the optical point of view, high transparency was observed and complex caustic patterns were created with LED light sources depending on the samples' geometry.

We believe the additive approach and glass printing technology has the capacity to democratize glass fabrication through its compact system design and ability to create custom structures with glass. Making with glass no longer need be limited to glass artists in rented studios and established glass manufacturers, but could be shifted into the hands of the masses.

Existing domains already affiliated with glass could have the opportunity to rapidly prototype with the material, and explore new potentials for its appealing properties. Since glass can be infinitely recycled without losing its material properties, glass bottles could be crushed locally instead of being sent back to a recycling plant, and processed into products. There is an abundance of silica on the planet (the primary constituent of glass) which lends itself to explore new product and manufacturing processes[43].

A few immediate applications could be explored by Industrial Designers, Artists, Architects and Scientists. Industrial designers could create novel lighting by establishing relationships between printed geometries and complex caustic patterns. Artists could explore the creation of novel multi-colored glass vessels with the platform and eliminate the expensive costs of glass studio time. Unitized mass-produced glass panels and blocks are ubiquitous in Architecture throughout the world. The platform could offer architects an expanded design space through customization and complexity for wall or roof tile systems. Scaling down the filament resolution to a smaller size (which would take a large amount of research and calibration) could make the technology a valuable piece of laboratory equipment for Scientists. Lab experiments are limited by the equipment they have, and the technology could alleviate this restriction. Microfluidic devices could also be explored assuming a feature size of 100 micron was able to be achieved.

Moving forward, the simultaneous development of the printer and the design of the printed glass objects will yield both a higher performance system and increasingly complex novel objects at finer resolutions. As such, applications in art, architecture and product design will be further explored while improvements such as continuous feeding, plunging, increased build size and start and stop control will be implemented in parallel.

The thesis offers exciting new directions for glass manufacturing and leaves an enormous amount of research to further be conducted. The Additive Manufacturing Enabling Technology for Optically Transparent Glass discovered new capabilities of this very challenging but limitless material, and is stepping stone in the rich, historic story of glass.

AUTHOR DISCOLOSURE STATEMENT

Klein, J., et al., Methods and apparatus for additive manufacturing of glass, U.S. Patent Application 14697564, filed April 27, 2015

REFERENCES

1. Gibson I, Rosen DW, Stucker B. Chapter 2: Development of Additive Manufacturing Technologies. In: Additive Manufacturing Technologies: Rapid Prototyping to Direct Digital Manufacturing. Springer Science + Business Media, LLC; 2010 p. 17–40.

2. ASTM. Standard Terminology for Additive Manufacturing Technologies. 2012;

3. Wohlers T, Caffrey T. Wohlers Report 2014. Fort Collins: Wohlers Associates; 2014.

4. Marchelli G, Prabhakar R, Storti D, Ganter M. The guide to glass 3D printing: developments, methods, diagnostics and results. Rapid Prototyp. J. 2011;17(3):187–194.

5. Zocca A, Colombo P, Gomes CM, Guenster J. Additive Manufacturing of Ceramics: issues, potentialities and opportunities. J. Am. Ceram. Soc. [in press];

6. Murr LE, Gaytan SM, Ramirez DA, et al. Metal Fabrication by Additive Manufacturing Using Laser and Electron Beam Melting Technologies. J. Mater. Sci. Technol. 2012;28(1):1–14.

7. Fateri M, Khosravi M. On-site Additive Manufacturing by Selective Laser Melting of composite objects. Concepts Approaches Mars Explor. 2012;

8. Klein S, Simske S, Parraman C, et al. 3D Printing of Transparent Glass. HP Tech Rep. 2012;

9. The Ex One Company L. The New Standard for Manufacturing from ExOne e Manufacturing in Sand.;

10. Clasen R. Method for the manufacture of glass bodies by extrusion. 1987;2–7.

11. Clasen R, Schmidl B. Method of manufacturing glass bodies by means of extrusion. 1989;

12. Eqtesadi S, Motealleh A, Miranda P, et al. Robocasting of 45S5 bioactive glass scaffolds for bone tissue engineering. J. Eur. Ceram. Soc. 2014;34(1):107–118.

13. Luo J, Pan H, Kinzel EC. Additive Manufacturing of Glass. J. Manuf. Sci. Eng. 2014;136(6):061024.

14. Bullseye Glass Co. The Vitrigraph Kiln - creating a new vocabulary in fused glass. 2014;(November):1–4.

15. Roeder E. Extrusion of glass. J. Non. Cryst. Solids 1971;5(5):377–388.

16. Fluegel A. Global model for calculating room-temperature glass density from the composition. J. Am. Ceram. Soc. 2007;90(8):2622–2625.

17. Fluegel A, Earl D a, Varshneya AK, Seward TP. Density and thermal expansion calculation of silicate glass melts from 1000 ° C to 1400 ° C. Phys. Chem. Glas. Eur. J. Glas. Sci. Technol. Part B 2008;49(5):245–257.

18. Vogel H. Das Temperaturabhängigkeitsgesestz der Viskosität von Flüssigkeiten. Phys. Z. 1921;22:645–646.

19. Tammann G, Hesse W. Die Abhängigkeit der Viskosität von der Temperatur bei unterkühlten Flüssigkeiten. Z. Anorg. Allg. Chem. 1926;156:245–257.

20. Fulcher GS. Analysis of recent measurements of the viscosity of glasses. J. Am. Ceram. Soc. 1925;8:339–355.

21. Bird RB, Stewart WE, Lightfoot EN. Transport Phenomena. Wiley; 1958.

22. Reynolds O. An experimental investigation of the circumstances which determine whether the motion of water shall be direct or sinuous, and of the law of resistance in parallel channels. Phil. Trans. R. Soc. Lond. 1883;174:935–982.

23. Chiu-Webster S, Lister JR. The fall of a viscous thread onto a moving surface: a "fluid-mechanical sewing machine." J. Fluid Mech. 2006;569:89.

24. Ribe NM. Coiling of viscous jets. Proc. R. Soc. A Math. Phys. Eng. Sci. 2004;460(2051):3223–3239.

25. Ribe NM, Habibi M, Bonn D. Liquid Rope Coiling. Annu. Rev. Fluid Mech. 2012;44(1):249–266.

26. Brun P-T, Audoly B, Ribe NM, et al. Liquid Ropes : A Geometrical Model for Thin Viscous Jet Instabilities. Phys. Rev. Lett. 2015;174501(May):1–5.

27. Mastelaro VR, Zanotto ED. Residual stresses in a soda-lime-silica. Joumal of Non-Crystalline Solids 1996;194:297–304.

28. Preston FW. The Use of Polariscopes in the Glass Industry [Internet]. J. Am. Ceram. Soc. 1930;13(9):595–623.

29. Belter JT, Dollar AM. Strengthening of 3D Printed Fused Deposition Manufactured Parts Using the Fill Compositing Technique. PLoS One 2015;10(4):e0122915.

30. Ahn S-H, Montero M, Odell D, et al. Anisotropic material properties of fused deposition modeling ABS. Rapid Prototyp. J. 2002;8(4):248–257.

31. Bertoldi M, Yardimci M a, Pistor CM, et al. Mechanical characterization of parts processed via fused deposition. Solid Free. Fabr. Proc. 1998;557–565.

32. Kim GD, Oh YT. A benchmark study on rapid prototyping processes and machines: quantitative comparisons of mechanical properties, accuracy, roughness, speed, and material cost. Proc. Inst. Mech. Eng. -- Part B -- Eng. Manuf. (Professional Eng. Publ. 2008;222(2):201–215.

33. Kiser T, Eigensatz M, Nguyen MM, et al. Architectural Caustics — Controlling Light with Geometry. Adv. Archit. Geom. 2012 2013;91–106.

34. Ashby, M. F. (2013). Materials and the Environment, Butterworth-Heinemann, Elsevier Inc, Oxford, UK.

35. Lowenstam, H. A. (2013). Minerals Formed by Organisms Science. Vol. 211: 1126-1131.

36. Vernadsky, V.I. (1967). Geochemistry and the Biosphere essays by Vladimir I. Vernadsky, Synergetic Press, Santa Fe.

37. Corning Museum of Glass, Ralph Appelbaum Associates (1999). Innovations in Glass, The Corning Museum of Glass. Upstate Litho, Rochester, New York.

38. Weaver, J. C., Milliron, G. W., Allen, P., Miserez, A., Rawal, A., Garay, J., ... Morse, D. E. (2010). Unifying Design Strategies in Demosponge and Hexactinellid Skeletal Systems. The Journal of Adhesion, 86(1), 72–95. doi:10.1080/00218460903417917

39. https://www.youtube.com/watch?v=DO7584g57z0 (Bullseye Glass Co. What is Glass? March 1, 2012).

40. http://www.youtube.com/watch?v=e907eCoFmCg (LaRouchePAC A Vernadskian Law of Evolution October 11, 2011 - Rouillard).

41. https://en.wikipedia.org/wiki/Glass (Glass, Wikipedia July 23, 2015).

42. https://www.youtube.com/watch?v=MD1BGuRrk9M (Glass Bulbs Ltd - The Ribbon Machine - 1950).

43. Kring, David A. Compositions of Earth's Continetal Crust as inferred from The Compositions of Impact Melt Sheets. Lunar and Planetary Science XXVIII. 1997; 1084.

FIGURE REFERENCES

Images and Figures that come from outside sources are listed below.

Figure 1A: Italmole S.N.C, Available online:
http://www.italmole.com/history_from_glass.htm
http://www.zuckershack.org/travel/egypt/
Figure 1B: Corning Museum of Glass, Available online:
http://www.cmog.org/article/pool-tin-float-glass
Figure 1C: Corning Museum of Glass, Available online:
http://www.cmog.org/collection/exhibitions/mirror-to-discovery
Figure 2A: North East Art Collective, Available online:
http://www.northeastartcollective.co.uk/?p=223
Figure 2B: Inhabitat, Available online:
http://inhabitat.com/rawlemon%E2%80%99s-spherical-solar-energy-generating-globes-can-even-harvest-energy-from-moonlight/andrebroessel2/
Figure 3: University of Cambridge, Material Selection and Processing, Available online:
http://www-materials.eng.cam.ac.uk/mpsite/interactive_charts/strength-density/NS6Chart.html
http://www-materials.eng.cam.ac.uk/mpsite/interactive_charts/strength-toughness/NS6Chart.html
http://www-materials.eng.cam.ac.uk/mpsite/interactive_charts/energy-cost/NS6Chart.html
Figure 4: Former Days, Available online:
http://www.formerdays.com/2012/03/crystal-palace.html
Figure 4: Diderot Encyclopedia, Glass. Available online:
http://www.mikegigi.com/diderot.htm
Figure 5: NSG Group, AGC Glass Europe. Available online:
http://www.glassforeurope.com/en/industry/float-process.php
Figure 6A: Lab Spaces, Institute of Physics. Available online:
http://www.labspaces.net/94608/Looking_through_Galileo_s_eyes

Figure 6B: History of the Microscope. Available online:
http://www.history-of-the-microscope.org/robert-hooke-microscope-history-micrographia.php

Figure 7A: University of Houston, Glass and Bottles. Available online:
http://www.uh.edu/engines/epi2155.htm

Figure 7B: National Park Service, The Electric Light System. Available online:
http://www.nps.gov/edis/learn/kidsyouth/the-electric-light-system-phonograph-motion-pictures.htm

Figure 8: Desktop Engineering. Available online:
http://www.deskeng.com/de/hot-trends-in-additive-manufacturing/

"Find purpose, the means will follow."
-Mahatma Gandhi